

NACA RM E54E13



RESEARCH MEMORANDUM

EFFECT OF UNEQUAL AIR-FLOW DISTRIBUTION FROM TWIN
INLET DUCTS ON PERFORMANCE OF AN AXIAL-FLOW
TURBOJET ENGINE

By Curtis L. Walker, Joseph N. Sivo, and Emmert T. Jansen

Lewis Flight Propulsion Laboratory
Cleveland, Ohio

CLASSIFICATION CHANGED

UNCLASSIFIED

LIBRARY COPY

AUG 5 1954

LANGLEY AERONAUTICAL LABORATORY
LIBRARY, NACA
LANGLEY FIELD, VIRGINIA

To: _____
By: authority of Diana TCA 9 *Effective* Date: 9-1-59

DB 11-20-59

CLASSIFIED DOCUMENT

This material contains information affecting the National Defense of the United States within the meaning of the espionage laws, Title 18, U.S.C., Secs. 793 and 794, the transmission or revelation of which in any manner to an unauthorized person is prohibited by law.

NATIONAL ADVISORY COMMITTEE FOR AERONAUTICS

WASHINGTON

August 3, 1954

~~CONFIDENTIAL~~
UNCLASSIFIED



UNCLASSIFIED

NATIONAL ADVISORY COMMITTEE FOR AERONAUTICS

RESEARCH MEMORANDUM

EFFECT OF UNEQUAL AIR-FLOW DISTRIBUTION FROM TWIN INLET DUCTS

ON PERFORMANCE OF AN AXIAL-FLOW TURBOJET ENGINE

By Curtis L. Walker, Joseph N. Sivo, and Emmert T. Jansen

SUMMARY

An investigation was conducted in an NACA altitude test chamber to determine the effect of inlet-air-flow distortion on the performance of an axial-flow turbojet engine having simulated twin inlet ducts. Data were obtained for the standard engine configuration and two inlet-air-flow distortion configurations for a range of engine speeds and exhaust-nozzle areas at Reynolds number indices of 0.6 and 0.2.

When the compressor was subjected to a circumferential inlet-air distortion such that each half of the compressor operated at a different inlet pressure, the performance point of each half of the compressor shifted along the constant corrected speed line of the performance map of the compressor with a standard inlet configuration. The corrected air flow for the half of the compressor operating at the lower inlet pressure was 2 to 3 percent lower than the corrected air flow for the compressor with a standard inlet. Because the air flow discharged from the compressor to essentially constant pressure, the pressure ratio of the portion of the compressor having the lower inlet pressure increased above the normal compressor pressure ratio while the pressure ratio of the other half of the compressor decreased. Stall of the compressor occurred at the condition where the pressure ratio across the portion of the compressor subjected to the lower inlet pressure reached the value at which stall occurred for the compressor with a normal inlet configuration.

A 37:63 percent air-flow division (compressor-inlet total-pressure difference of 32 percent) between the twin inlet ducts resulted in a decrease in maximum thrust of about 10 percent at 22,000 feet and 25 percent at 50,000 feet at a flight Mach number of 0.6. If the engine performance is based on 100-percent ram recovery in the unblocked duct instead of average pressure at the compressor inlet (thus charging the installation with the loss in the blocked duct), the thrust loss is approximately 23 percent at the low altitude and approximately 35 percent at the high altitude. The more severe thrust loss at high altitude resulted from the blocked portion of the compressor encountering the stall region, which made it necessary to limit operation of the engine to less than rated speed.

UNCLASSIFIED

13301

CR-1

INTRODUCTION

Nonuniform distribution of pressure and air flow at the inlets to turbojet engines, caused by the inlet ducting or combat maneuvering of the aircraft, may result in large engine performance losses. As was noted in reference 1, an unequal air-flow division and discontinuity in total pressure at the compressor inlet can result in a decrease in thrust and an increase in specific fuel consumption because of a reduction in compressor air flow and reduced component efficiencies. It is also possible that unequal air-flow distributions may cause rotating stall or surge with possible damage to the compressor or turbine because of excessive blade vibrations (ref. 2). A general NACA research program is being conducted to determine the effect of these air-flow distortions on the component and over-all performance of several engines. As a part of this program, an investigation was made to determine the effects on engine performance of unequal air flow distribution through simulated twin inlet ducts. The effect of inlet air distortion on compressor blade vibration and compressor rotating stall was also investigated. The unequal air flow through the two branches of the duct discharged separately at the compressor inlet. The engine used in this investigation was a current production-model turbojet engine.

The simulated twin-inlet-duct distortions investigated consisted of nominal air flow divisions between the two ducts of 45 and 55 percent and of 40 and 60 percent. These distortions were obtained by inserting fine mesh screens in one of the inlet ducts. The most severe distortion (40:60) corresponded to the extreme condition expected during maneuvering for a similar inlet in a proposed high-speed missile.

The compressor, turbine, and over-all engine performance with distortion was compared with performance without distortion. At Reynolds number indices of 0.6 and 0.2, data were obtained at corrected engine speeds of 60, 80, 88, 95, 100, and 107 percent of rated speed over a range of engine temperature ratios. These Reynolds number indices are equivalent to inlet conditions corresponding to a range of flight conditions; for example, a Reynolds number index of 0.6 corresponds to an altitude of 22,000 feet and flight Mach number of 0.6, while a Reynolds number of 0.2 corresponds to an altitude of 50,000 feet at the same flight Mach number.

APPARATUS

Engine

A schematic sketch of the turbojet engine used in this investigation as it was installed in one of the NACA Lewis altitude test chambers is shown in figure 1. This engine had a 12-stage axial-flow compressor, eight can-type combustors, and a single-stage turbine. The sea-level static thrust rating of the engine is 5970 pounds at a rated speed of 7950 rpm and turbine-outlet temperature of 1735° R.

A view of the bellmouth inlet showing the splitter plate used to divide the inlet into two ducts is shown in figure 2. This splitter plate extended from the entrance of the bellmouth to the forward bearing strut. This strut in turn extended to within 1/4 inch of the inlet guide vanes. Thus the inlet simulated the type of twin-duct installation where the two ducts discharge directly into the compressor inlet.

A typical screening configuration is also shown in figure 2. A 1/4-inch mesh screen was placed over the entire annulus approximately 37 inches upstream of the inlet guide vanes. A fine screen was then supported on the quarter-inch mesh in one half of the inlet to effect the desired distortion.

The configurations and sizes of the fine mesh screen are described in the following table:

Configuration	Nominal air-flow division	Size of screen	
		Unblocked duct	Blocked duct
A	50 - 50	$\frac{1}{4}$ "	$\frac{1}{4}$ "
B	45 - 55	$\frac{1}{4}$ "	$\frac{1}{4}$ " + 40 mesh
C	40 - 60	$\frac{1}{4}$ "	$\frac{1}{4}$ " + 60 mesh

Instrumentation

Instrumentation for measuring temperatures and pressures was installed at stations indicated in figure 1. Details of the instrumentation stations are shown in figure 3. In addition, there were two wall static-pressure taps in each of the first 11 compressor rotor rows. These rows of orifices were located diametrically opposite each other in a plane perpendicular to the splitter plate. Four nozzle lip static probes were installed to determine the exhaust-nozzle-discharge static pressure. Strip recorders were installed to record engine-inlet total pressure, compressor-outlet total pressure, engine speed, and turbine-outlet total pressure and temperature during engine transient operation resulting from throttle bursts to determine the stall characteristics of the engine.

A magnetic pickup, shown in figure 4, was installed in the compressor for detecting vibration of the first-stage compressor rotor

1055

CR-1 back

blades. The magnetic flux path, energized by the permanent magnet, passes down the core, across the air gap, and through the outside shell of the magnet. Whenever a magnetic material is moved in the air-gap flux, the resultant flux change produces a voltage in the coil proportional to the rate of change of flux which depends in part on the following: the nature of the material passing through the flux, the velocity with which the material passes, the position of the material in the gap flux, and the shape of the material. The variation of signal amplitude with material position was utilized in this application.

The pickup was mounted in the compressor case in such a manner that the leading edge of the rotor blades lay in the same plane as the trailing edge of the pickup; thus a voltage pulse was produced by each blade tip as the rotor revolved. These voltage pulses were displayed on an oscilloscope with the sweep recurrence synchronized with the rotor rotations, and a stationary pattern was observed consisting of one voltage pulse for each blade passage. If, however, a blade were vibrating (vibration frequency is not an even multiple of the speed of the rotor), the amplitude of signal produced by the vibrating blade would fluctuate about the amplitude that would be produced if the blade were not vibrating.

Constant-temperature hot-wire anemometers were used for detection of flow fluctuations caused by rotating stall. The anemometer probes used were wired with 0.0002-inch-diameter tungsten wire with an unplated length (effective length) of 0.08 inches. The wire element was mounted perpendicular to the probe axis. Four of these anemometer probes, located at 90° circumferential intervals, were installed in radial survey devices in the compressor fourth-stage stator.

Procedure

Engine performance data were obtained at the conditions described in the following table. The temperatures, pressures, and engine speed given are average values. The total pressure listed is the mass-averaged compressor-inlet pressure used in the calculations.

3301

Reynolds number index	Engine-inlet total temperature, T_1 , OR	Compressor-inlet total pressure, P_2 , lb/sq ft	Engine speed, rpm	Corrected engine speed, $N/\sqrt{\theta}$, percent of rated
Configuration A				
0.6	533	1302	4824	60
	457	1026	6544	88
	458	1007	7068	95
	459	1011	7465	100
	410	868	7546	107
0.2	412	302	6224	88
	413	301	6745	95
	422	302	7160	100
	416	288	7570	107
Configuration B				
0.6	535	1285	4825	60
	462	971	6582	88
	461	858	7108	95
	424	830	7136	100
	419	814	7608	107
0.2	535	293	6275	88
	415	280	6753	95
	411	282	7147	100
	417	272	7588	107
Configuration C				
0.6	532	1270	4805	60
	458	930	6545	88
	422	816	6756	95
	452	884	7415	100
	417	788	7655	107
0.2	423	286	6325	88
	417	278	6803	95
	420	267	7100	100
	---	---	----	107

A range of exhaust-gas temperature for each condition was obtained by closing the nozzle flaps until limiting exhaust-gas temperature or compressor stall or surge was reached. At a Reynolds number index of 0.2 and corrected engine speed $N/\sqrt{\theta} = 107$ percent for configuration B, only wide open nozzle operation was possible because of temperature limits. At the same index and speed for configuration C stall was encountered when an attempt was made to reach this condition. After a failure of the turbine, which will be discussed in RESULTS AND DISCUSSION, operation was arbitrarily limited by a combustor-outlet (turbine-inlet) temperature of 2260° R as indicated by single thermocouples located in the center of each burner transition (station 4, figs. 1 and 3(d)).

Compressor stall lines were determined by using a continuous strip recorder during engine throttle bursts to record compressor pressure ratio and engine speed. With configuration C at high altitude it was also possible to obtain stall by slowly closing the exhaust-nozzle flaps so that steady-state instrumentation could be used for determining some stall points.

A mass-averaged inlet total pressure was used in determining the correction factor δ . The symbols used in this report are defined in appendix A and the methods of calculation are described in appendix B.

RESULTS AND DISCUSSION

Pressure and Temperature Profiles

In order to illustrate the magnitude of the distortions used, the percentage of total engine air flow passing through the unblocked duct is presented in figure 5 for configurations B and C. Configuration B had an air flow division of 43:57 percent at the higher corrected engine speeds while configuration C had an air flow division of 37:63 percent. The exceptions to these values are the data for a corrected engine speed of 60 percent of rated. The data indicate that the low Mach number at the screen associated with the low engine speed caused a relatively lower pressure drop across the fine-mesh screen and, hence, a more nearly equal air-flow distribution than at the higher engine speed.

Typical compressor pressure and temperature profiles at a given engine speed are presented in figure 6 for the three configurations investigated. The ordinate was obtained by first dividing the individual probe value by the average value in order to put all profiles on a comparative basis and, second, dividing this ratio by a similar probe ratio for the undistorted condition to eliminate small circumferential variations in the undistorted profiles. This same procedure was used for

all the circumferential profiles. The abscissa is the circumferential location of the probes measured counterclockwise from the top looking downstream. The splitter plate location was at 135° and 315° (see figs. 2 and 3(b)). The high-pressure region or unblocked duct extended from 315° to 135° and the low-pressure region or blocked duct from 135° to 315° .

3301 The total-pressure profiles at the compressor inlet and outlet are presented in figures 6(a) and 6(b), respectively, for the same data points. The difference between the maximum and the minimum pressure has been reduced from about 20 and 32 percent at the compressor inlet to about 5.0 and 6.5 percent at the compressor outlet for configurations B and C, respectively. The circumferential location of the splitter at the compressor inlet is indicated on figure 6(a). Figures 6(a) and 6(b) indicate that while the low-pressure area at the compressor inlet subtended the angle from 135° to 315° , the low-pressure region rotated about 60° in the direction of compressor rotor rotation and subtended the angle from 195° to 15° at the compressor outlet.

The compressor-outlet temperature in the blocked side is higher than that in the unblocked side (fig. 6(c)) because of the increased compressor pressure ratio and likewise subtends about the same angle as the compressor-outlet low-pressure area.

The effect of engine speed on the distortion of compressor-inlet and -outlet total pressure and temperature profiles is shown in figure 7. As the engine speed is decreased, the velocity of the air at the engine inlet decreased so that for a given screen configuration the pressure distortion at the engine inlet decreases, resulting in decreased effects of the compressor outlet. The effect of Reynolds number index on these pressure and temperature profiles is shown in figure 8. Decreasing the Reynolds number index from 0.6 to 0.2 had no effect on pressure distortions at the compressor inlet and outlet but tended to create more severe temperature gradients at the compressor outlet.

Turbine-inlet total-temperature profiles were not available because of inadequate instrumentation at station 4. (The instrumentation at that station was used only as an indication of excessive temperature at the turbine inlet.) Turbine-outlet total-temperature profiles based on individual rake averages are presented in figure 9 for the same data points presented in figure 6. This large circumferential variation in temperature profile at the turbine outlet results mainly from the severe circumferential variation in fuel-air ratio caused by maldistribution of air flow. No radial turbine-outlet temperature profile shift was discernible from these limited measurements.

Component Performance

Compressor. - The effect of circumferential inlet-air distortion on compressor performance is presented in figures 10 to 14. With distortion, the exact amount of air flow passing through each half of the compressor is extremely difficult to determine because of cross flow between the outlet of the splitter plate and the inlet of the compressor due to the large circumferential static pressure gradient. (The static-pressure gradient is of the same magnitude as the total-pressure gradient.) In addition, there is probably cross flow and mixing within the compressor itself. Because of this cross flow, it is not entirely correct to assign the air flow as measured in each of the two ducts to the corresponding half of the compressor.

However, to serve as a starting point in the analysis of the behavior of the compressor during air distortion, the compressor maps based on the air flows as measured in the ducts for the three configurations investigated are presented in figure 10 for two Reynolds number indices. The inlet pressure used to calculate the pressure ratio and to correct the air flow through each duct is the mass flow average in each of the two ducts. The air flow in each duct has been multiplied by two in order to put them on a comparable basis with the standard compressor. The compressor-outlet pressure was calculated taking into account the circumferential shift in pressure profiles exhibited in figure 6. Lines of constant compressor efficiency for configuration A have been superimposed on the figures representing a Reynolds number index of 0.6.

As the compressor is subjected to a circumferential inlet air distortion, the blocked half of the compressor operates at higher compressor pressure ratios than the standard compressor configuration, while the unblocked half operates at lower pressure ratios. As the amount of distortion is increased, the pressure ratio across the blocked half of the compressor increases and moves toward the stall region, while the pressure ratio across the unblocked half remains relatively unchanged. At a Reynolds number index of 0.2, engine operation with configuration C was impossible at a speed of 107 percent of rated because compressor stall was encountered over the entire range of exhaust-nozzle areas covered.

Because of the uncertainty in the actual air flow through each half of the compressor, the displacement of the constant-speed lines on the compressor map may be exaggerated in figure 10. As an engine is subjected to air distortions, the undistorted portion of the compressor would be expected to operate about the same as it did before the distortion occurred. Therefore, the increase in air flow in the unblocked duct may be considered to be an indication of the amount of cross flow from the unblocked to the blocked portion of the compressor. If it is assumed

that the unblocked half of the compressor operates in a normal manner, the air flow of the unblocked half may be determined from the undistorted compressor performance maps (configuration A) by using the corrected engine speed and compressor pressure ratio across the unblocked half. The difference between the air flow measured in the unblocked duct and the air flow through the unblocked half of the compressor may be applied to the air flow as measured in the blocked duct to obtain an air flow for the blocked half of the compressor.

In order to verify the assumption made that the unblocked portion of the compressor operates in a normal manner, the efficiency of the unblocked half of the compressor was compared with the efficiency of the standard compressor (configuration A). For the same compressor pressure ratio and engine speed, the variations between the two efficiencies were generally less than 0.01 for the range of conditions investigated (fig. 11(a)).

By means of the procedure described in the previous two paragraphs, a second performance map was constructed based on the adjusted air flows through each half of the compressor and is presented in figure 11(b) for a Reynolds number index of 0.6. The adjusted air flow of the blocked half of the compressor appears to be 2 to 3 percent lower than would be expected for the undistorted compressor configuration. This may be a result of the indeterminable effect of cross flow and mixing on this portion of the compressor. However, where figure 10(a) showed the blocked portion of the compressor for configuration C to be operating in the region of stall, figure 11 shows the blocked portion of the compressor to be operating at a considerable distance from stall except at the higher corrected engine speeds. The adjusted performance of the compressor at a Reynolds number index of 0.2 exhibited similar trends as the performance at a Reynolds number index of 0.6.

The average over-all performance of the compressor is presented in figure 12 for two engine speeds and Reynolds number indices in order to provide air flow and pressure ratio quantities which are readily usable for engine performance calculations. The compressor-inlet total pressure which is used to correct the air flow and to obtain the compressor pressure ratio is the combined mass-averaged compressor-inlet total pressure of both ducts. Varying the air flow divisions from 50:50 to 37:63 percent between the two ducts at a given average exhaust-gas temperature results in a 4 to 5 percent decrease in over-all air flow and compressor pressure ratio. Figure 12(a) includes two sets of constant corrected average exhaust-gas temperature lines to show the shift to higher compressor pressure ratios as the inlet air distortion is increased. This upward shift is a result of a loss in component efficiencies. At the lower Reynolds number index, engine operation was restricted to lower average exhaust-gas temperature as the distortion was increased in order to keep the blocked portion of the compressor from operating in the stall region.

The effect of air flow distortion on the compressor stall characteristics is shown in figure 13 for a Reynolds number index of 0.6 for the three configurations investigated. The data in this figure were obtained from both transient instrumentation used during throttle bursts and steady-state instrumentation. The transient instrumentation was inadequate to provide air flow at stall; therefore, the stall lines have been represented as a plot of compressor pressure ratio against corrected engine speed. The compressor pressure ratio data points on the figure for configurations B and C represent the pressure ratio across the blocked half of the compressor. Also presented on this figure are constant exhaust-nozzle-area lines for the three configurations investigated to show the large reduction in accelerating margin as the distortion is increased.

At any given engine speed, stall of the compressor subjected to inlet distortions occurs at the condition where the pressure ratio of the distorted portion of the compressor equals the stall pressure ratio of the undistorted compressor (configuration A). Therefore, if the amount of distortion at the engine inlet and associated pressure gradient is known, a fairly accurate calculation can be made to determine whether stall will be encountered for any particular engine and flight operating condition.

For the range of configurations investigated, the effect of inlet air distortion on the over-all compressor efficiency at Reynolds number index of 0.6 was negligible for all engine speeds except at a corrected engine speed of 107 percent (fig. 14(a)). At this speed, the loss in over-all compressor efficiency for configuration C was about 0.07. At a Reynolds number index of 0.2, increasing the inlet distortion resulted in a decrease in over-all compressor efficiency for all engine speeds investigated; the efficiency losses of about 0.07, 0.06, and 0.02 occurred at the corrected engine speeds of 100, 95, and 88 percent, respectively (fig. 14(b)).

The compressor efficiencies for each half of the compressor are compared in figure 15 for the two air flow distortion configurations. Inspection of the data showed that for configuration B, the air flow distortion had very little effect on the compressor efficiency for each half of the compressor as compared to the over-all compressor efficiency. For configuration C, a compressor efficiency calculated for the unblocked half of the compressor was 1 to 5 points higher than the efficiency for the blocked half.

Turbine. - The effect of distortion on turbine efficiency at both Reynolds number indices was negligible (fig. 16). The accuracy of determination of turbine efficiency is such that the apparent discernible trends are not reliable. The changes in turbine efficiency

may be considerably less important than the effects of circumferential temperature and pressure gradients on the stress levels and fatigue life of the turbine stator and rotor.

Combustor. - Because of a lack of sufficient instrumentation, combustor efficiency could not be obtained for each can-type combustor. However, calculations across the entire engine indicated no noticeable effect of inlet air distortion on combustor efficiency for the range of conditions covered. Combustor efficiency would not be expected to show any appreciable change due to inlet air distortions because the compressor-outlet circumferential pressure gradients and thus air flow gradients were not severe.

Over-All Engine Performance

Engine pumping characteristics. - The effect of distortion on engine pumping characteristics is shown in figure 17 at Reynolds number indices of 0.6 and 0.2. The engine-inlet total pressure is the combined mass-averaged compressor-inlet total pressure of both ducts. For a given engine speed and temperature ratio, increasing the inlet air distortion decreases the engine pressure ratio because of the loss in compressor efficiency and the reduction in compressor pressure ratio.

Net thrust and specific fuel consumption. - The effect of inlet air distortion on net thrust and specific fuel consumption is shown in figure 18 based on an average exhaust-gas temperature of 1760° R irrespective of turbine-inlet temperature gradients. It is apparent that if a temperature limit was imposed at the turbine inlet which prevented engine operation on an average exhaust-gas temperature, a further loss in thrust would be encountered for any given inlet air distortion.

Because there are two bases for determining engine ram-pressure ratio, a comparison of thrust and specific fuel consumption was made for the two methods and is presented for an altitude of 22,000 feet and flight Mach number of 0.6, corresponding to a Reynolds number index of 0.6. The solid line on this figure was based on average pressure at the compressor inlet; that is, the assumption is that the average ram-pressure recovery is 100 percent. This assumption is the same as was used in reference 1 and provides a basis for examining the loss in thrust due only to decreased component efficiency and air flow. This thrust loss was approximately 10 percent at an altitude of 22,000 feet (fig. 18(a)) for configuration C (37:63 air flow division).

The dashed line on figure 18 is based on 100 percent ram-pressure recovery in the unblocked duct. This assumption provides a comparison of thrust loss which includes the pressure loss in the blocked duct

10301

CR-2 back

required to effect the distortion. Comparison on this basis shows a 23 percent loss in thrust at an air flow division of 37:63 percent. The decrease in net thrust was accompanied by a proportional increase in specific fuel consumption.

The engine speed and average exhaust-gas temperature must be reduced at high altitude and high distortion to prevent compressor stall. Therefore, if the engine were equipped with a control which maintained constant speed and average exhaust-gas temperature and encountered a distortion of a magnitude corresponding to configuration C, compressor stall would occur if the original operation had been at rated speed and temperature. If, on the other hand, distortion was anticipated, an engine equipped with this type of constant-speed, constant-temperature control would require a 13 percent thrust derating in the undistorted case (fig. 19) to provide stall-free operation up to an air flow division of 37:63 percent. The performance is based on 100 percent ram-pressure recovery in the unblocked duct for an altitude of 50,000 feet and flight Mach number of 0.6, which corresponds to a Reynolds number index of 0.2. The over-all reduction in thrust due to the distortion of configuration C was approximately 33 percent at 50,000 feet. The net thrust specific fuel consumption presented indicates that the derating in thrust improved the specific fuel consumption because of higher component efficiency at the lower-speed operation.

Operational Comments

Compressor rotating stall was detected at only one operating condition during this investigation. It occurred with configuration C at rated corrected engine speed and exhaust-gas temperature at a Reynolds number index of 0.2. The signal from the hot-wire anemometers indicated a frequency of 56.3 cycles per second. One stall region was assumed to exist, which leads to the conclusion that it was rotating at about 45 percent of engine speed. The oscillograph of the hot-wire signal is shown in figure 20. About 10 to 20 seconds after this condition was established, the turbine failed. The stator (fig. 21(a)) was badly burned in the area corresponding to the high-temperature area of the profiles discussed previously. Failure of the turbine stator or deterioration of compressor performance due to progressive increase of the stall in the latter stages resulted in a tendency for speed to decrease. Because the engine was equipped with a constant-speed control, the increase in fuel flow and turbine-inlet temperature introduced by the control resulted in the failure of the turbine rotor (fig. 21(b)) in a short time. This was a single failure and the results are not conclusive; however, the severe temperature profiles discussed earlier present an undesirable condition with distortions of this magnitude. This failure indicated that should such a severe distortion occur at high altitude during a maneuver,

compressor stall would be encountered which might lead to engine failure within a matter of seconds. Derated operation mentioned previously and indicated on figure 19 is a possible means of preventing failure for distortions up to an air flow division of 37:63 percent, at 50,000 feet and a Mach number of 0.60.

No vibrations of the first-stage rotor blades of appreciable amplitude were observed during the program.

CONCLUDING REMARKS

An investigation was conducted to determine the effects on performance of an axial-flow turbojet engine of unequal air flow through simulated twin inlet ducts. The division in air flow resulted in a discontinuous total-pressure profile at the compressor inlet. The magnitude of the total-pressure profile diminished in passing through the compressor. However, a temperature gradient appeared at the compressor outlet and its magnitude increased in passing through the combustors and turbine.

The corrected air flow of the blocked half of the compressor is about 2 to 3 percent lower than would be expected for the undistorted compressor configuration; this is believed to be caused by the cross flow and mixing due to inlet air distortions. The portion of the compressor subjected to the distortions operates at higher pressure ratio than the standard compressor configuration, while the undistorted portion operates at lower pressure ratios. At any given engine speed, stall of the compressor subjected to circumferential inlet distortions occurs at the condition where the pressure ratio of the distorted portion of the compressor equals the stall pressure ratio of the undistorted compressor configuration.

The most severe distortion investigated was a 37:63 percent air flow division between the two ducts. This distortion resulted in a maximum loss in compressor efficiency of about 0.07 and a decrease in total air flow of about 7 percent at a corrected engine speed of 107 percent. As a result, the thrust decreased about 10 percent at an altitude of 22,000 feet at a flight Mach number of 0.6 (where flight condition was based on average compressor-inlet pressure). If the flight conditions are based on 100 percent ram-pressure recovery in the unblocked duct (thus charging the installation with the pressure loss in the blocked duct necessary to effect the distortion), the thrust losses are approximately 23 and 35 percent at a flight Mach number of 0.6 and altitudes of 22,000 and 50,000 feet, respectively. Part of the thrust loss at the higher altitude was due to the necessary reductions in engine speed and exhaust-gas temperature in order to avoid compressor stall.

At high altitudes, unless engine speed and exhaust gas temperature are reduced, the inlet air distortion may result in circumferential temperature gradients at the turbine severe enough to cause turbine failures.

Lewis Flight Propulsion Laboratory
National Advisory Committee for Aeronautics
Cleveland, Ohio May 17, 1954

APPENDIX A

SYMBOLS

The following symbols are used in this report:

A	area, sq ft
F_n	net thrust, lb
f	fuel-air ratio
g	acceleration of gravity, ft/sec ²
M	Mach number
N	engine speed
P	total pressure, lb/sq ft
p	static pressure, lb/sq ft
R	gas constant, ft-lb/(lb)(°R)
T	total temperature, °R
V	velocity, ft/sec
W	air flow, lb/sec
W_f	fuel flow, lb/hr
γ	ratio of specific heats
δ	ratio of engine-inlet total pressure P_1 to NACA standard sea-level pressure, 2116 lb/sq ft
θ	ratio of engine inlet total temperature T_1 to NACA standard sea level temperature, 519° R
η	efficiency
ϕ	ratio of coefficient of viscosity corresponding to T_1 to coefficient of viscosity corresponding to NACA standard sea-level temperature, 519° R. This ratio is a function of only temperature and is equal to $735 \theta^{1.5} / (T + 216)$.
$\frac{\delta}{\phi \sqrt{\theta}}$	Reynolds number index

Subscripts:

- a unblocked duct
- b blocked duct
- c compressor
- j vena contracta at exhaust nozzle outlet
- CL compressor leakage air flow
- t turbine

Station numbers:

- 0 ambient or free-stream conditions
- 1 engine inlet
- 2 compressor inlet
- 3 compressor outlet or combustor inlet
- 4 combustor outlet or turbine inlet
- 5 turbine outlet
- 9 exhaust-nozzle inlet

APPENDIX B

METHODS OF CALCULATION

Compressor-inlet total pressure. - The total pressure in each duct was determined by the indicated pressure on a seven-probe rake located approximately 3 inches ahead of the inlet guide vanes. The average pressure was determined by

$$P_2 = \frac{W_{1,a} P_{2,a} + W_{1,b} P_{2,b}}{W_{1,a} + W_{1,b}}$$

The correction factor δ was calculated from this mass-averaged pressure.

Engine air flow. - The air flow was determined in each duct from the temperature and pressures at station 1 by the equation

$$W_{1,a} = A_{1,a} P_{1,a} \sqrt{\frac{2\gamma_1}{\gamma_1 - 1} \frac{g}{RT_1} \left[\left(\frac{P_{1,a}}{P_{1,a}} \right)^{\frac{\gamma_1 - 1}{\gamma_1}} - 1 \right] \left(\frac{P_{1,a}}{P_{1,a}} \right)^{\frac{\gamma_1 - 1}{\gamma_1}}}$$

for the unblocked duct and a similar equation for the blocked duct.

The total corrected air flow was defined as $\frac{(W_{1,a} + W_{1,b}) \sqrt{\theta}}{\delta}$ where θ is the same for both ducts since the compressor-inlet total temperature was uniform.

Compressor and turbine efficiencies. - The compressor and turbine efficiencies were calculated from conventional adiabatic equations. Except for mass-averaged compressor-inlet total pressure, all pressures and temperatures were arithmetic averages.

Net thrust. - In the determination of net thrust, the following items were assumed: (1) altitude (NACA standard atmosphere); (2) flight Mach number; (3) exhaust-gas temperature, T_9 ; and (4) corrected engine speed, $N/\sqrt{\theta}$.

The first two of these items define P_1 , T_1 , p_0 , V_0 , δ , and θ . Compressor-inlet total temperature T_1 and item (3) determine engine temperature ratio T_9/T_1 . From engine pumping characteristics (fig. 17) and corrected engine temperature ratio T_9/T_1 , the engine pressure ratio P_9/P_2 was determined. Compressor pressure ratio P_3/P_2 was

determined from a plot of compressor pressure ratio as a function of T_9/T_1 . From P_3/P_2 , $N/\sqrt{\theta}$, and figure 12, the corrected air flow

$\frac{W_a \sqrt{\theta}}{\delta}$ was determined. The thrust equation was

$$F_n = \left\{ (1+f)(W_{a,1} - W_{CL}) V_j + A_j (P_j - P_0) \right\} - \frac{W_{a,1} V_0}{g}$$

The part of this equation enclosed by braces can be solved by use of the effective velocity parameter of reference 3, W , T_9 , γ_9 , and P_0/P_9 . The compressor leakage air flow, W_{CL} was determined from P_3 and figure 22. Engine fuel-air ratio f was determined using T_9/T_1 , θ , and figure 23.

Specific fuel consumption. - The net thrust specific fuel consumption was determined from the following equation:

$$\text{sfc} = \frac{W_f}{F_n}$$

REFERENCES

1. Wallner, Lewis E., Conrad, E. William, and Prince, William R.:
Effect of Uneven Air-Flow Distribution to the Twin Inlets of an Axial-Flow Turbojet Engine. NACA RM E52K06, 1953.
2. Huppert, Merle C., Costilow, Eleanor L., and Budinger, Ray E.:
Investigation of a 10-Stage Subsonic Axial-Flow Research Compressor. III - Investigation of Rotating Stall, Blade Vibration, and Surge at Low and Intermediate Compressor Speeds. NACA RM E53C19, 1953.
3. Turner, L. Richard, Addie, Albert N., and Zimmerman, Richard H.:
Charts for the Analysis of One-Dimensional Steady Compressible Flow. NACA TN 1419, 1948.

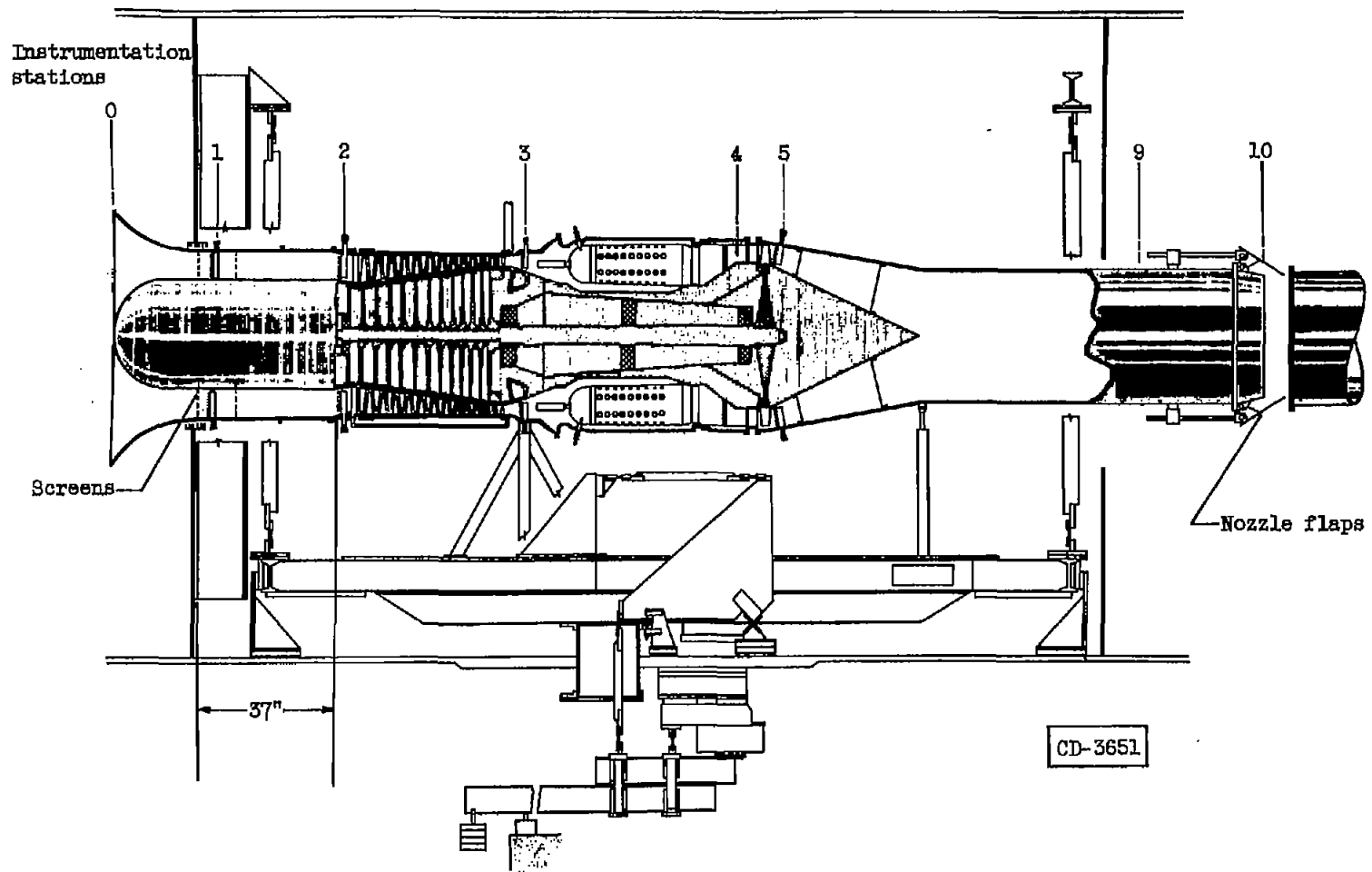
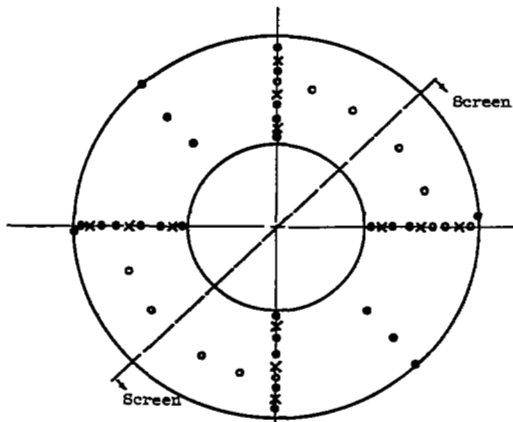


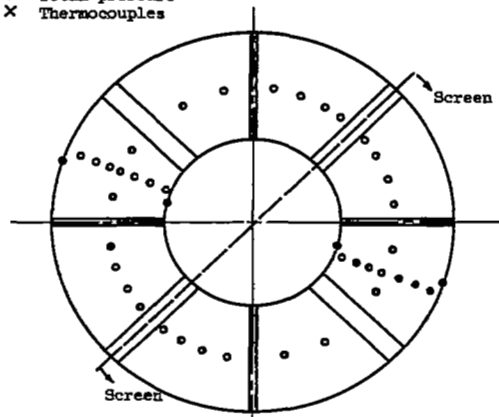
Figure 1. - Schematic diagram of engine installation in altitude test chamber showing location of instrumentation stations.

3301

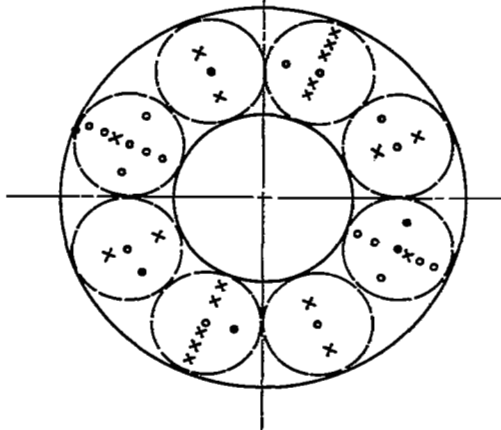
● Static pressure
○ Total pressure
× Thermocouples



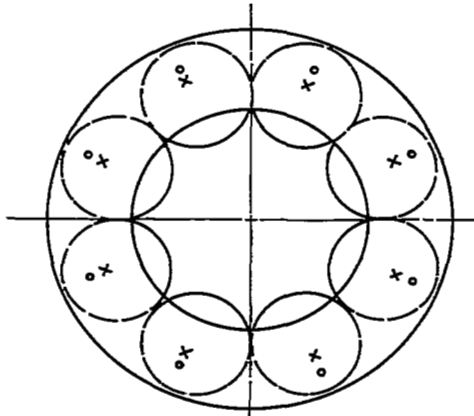
(a) Station 1, bellmouth inlet (air-flow measuring station in straight section of duct).



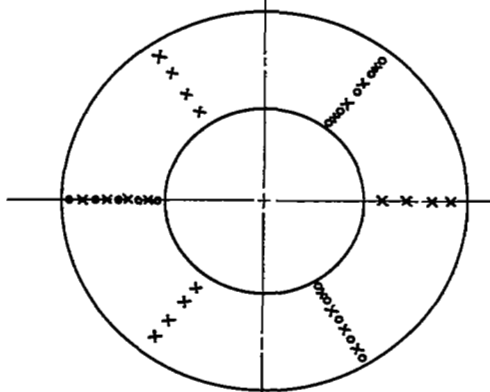
(b) Station 2, compressor inlet.



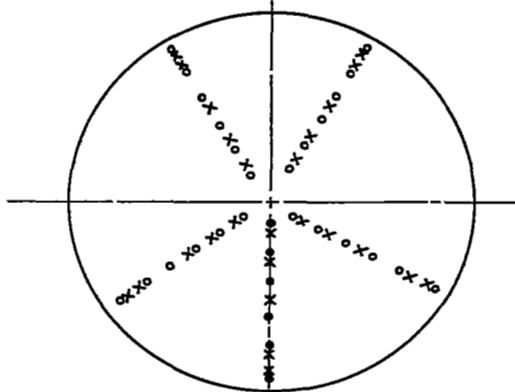
(c) Station 3, compressor outlet.



(d) Station 4, turbine inlet.



(e) Station 5, turbine outlet.



(f) Station 9, exhaust-nozzle inlet.

Figure 3. - Instrument station details for investigation of inlet-air distortion (looking downstream).

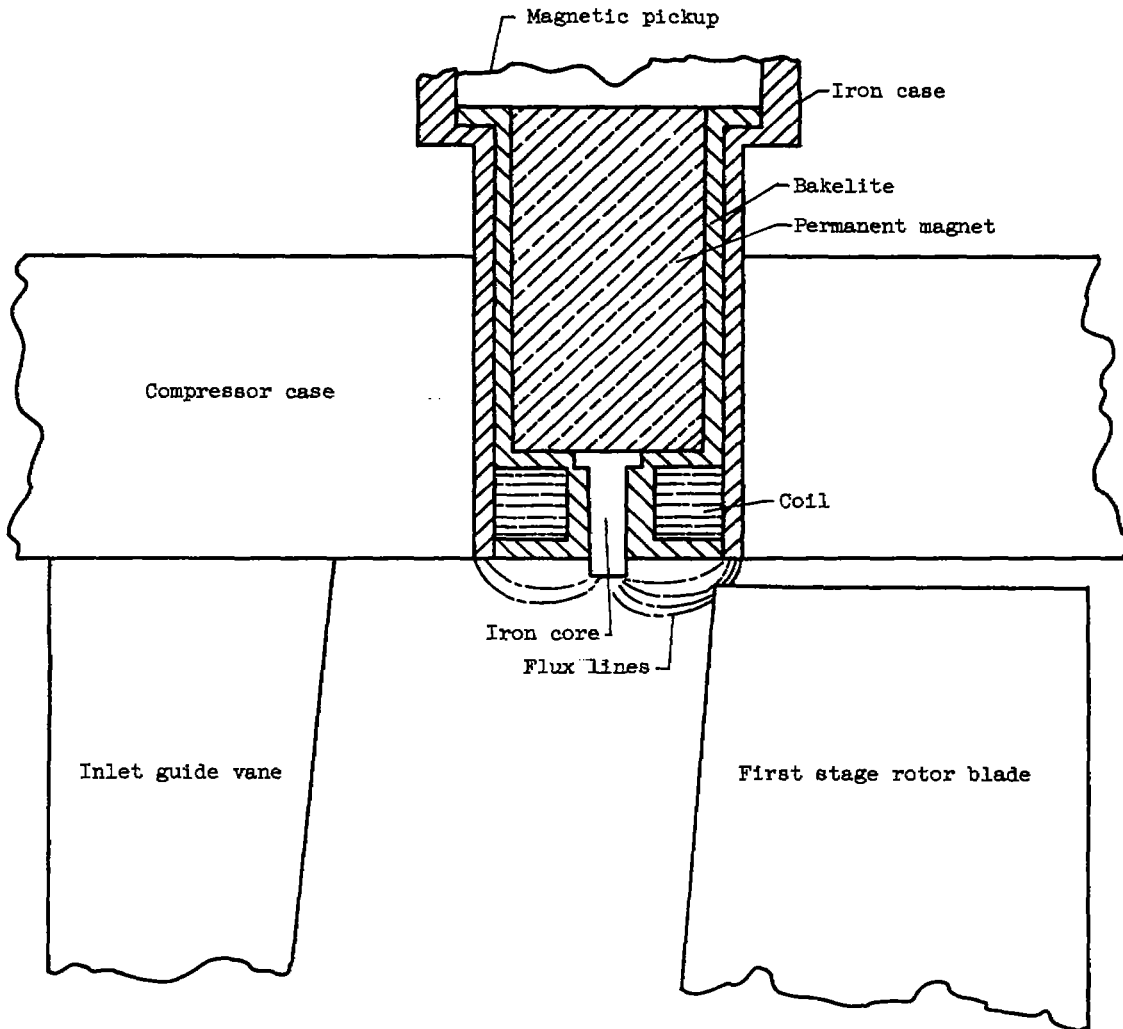


Figure 4. - Sketch of magnetic pickup used for detection of vibration of first stage compressor rotor blades.

3301

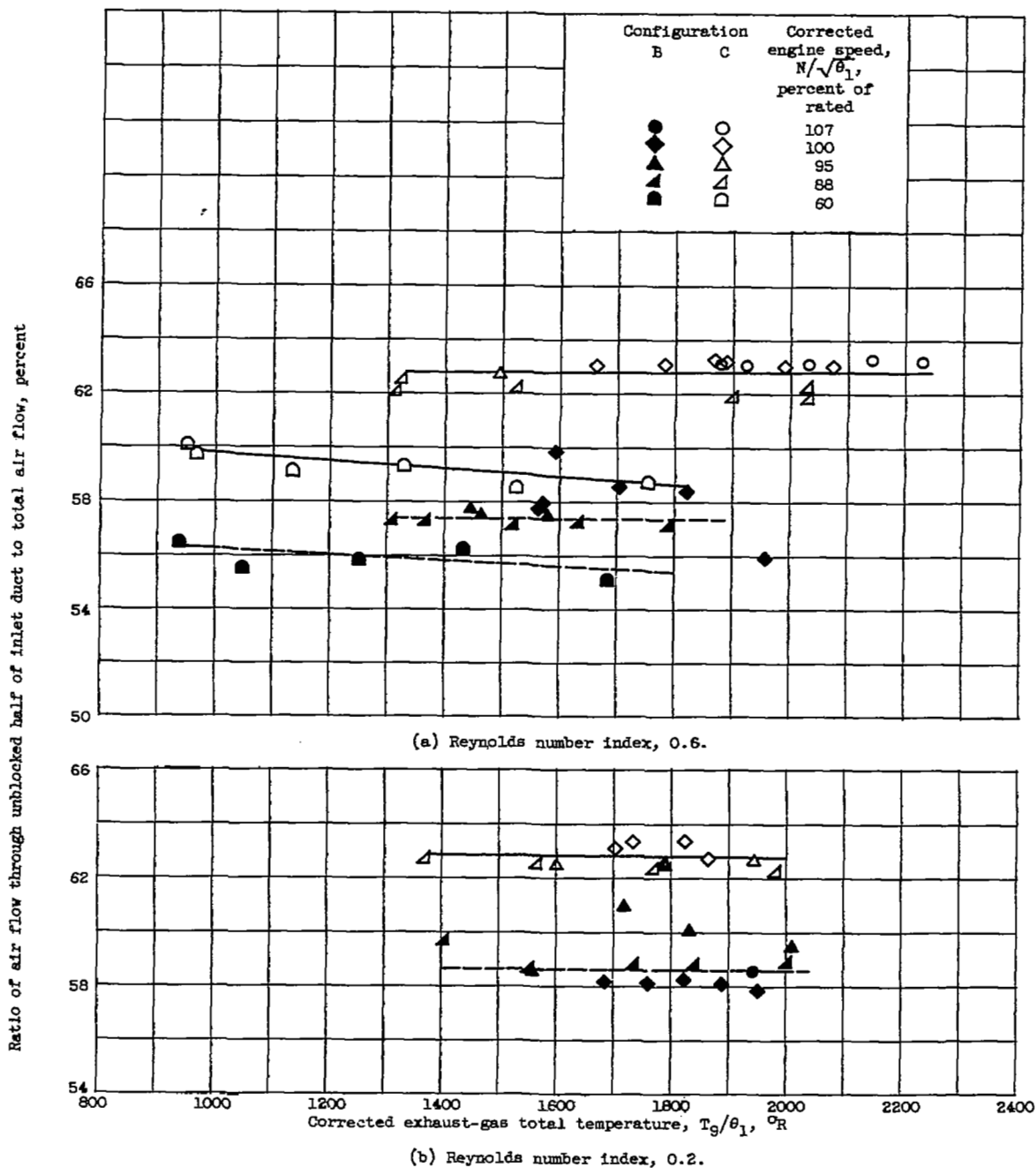


Figure 5. - Air flow through unblocked duct.

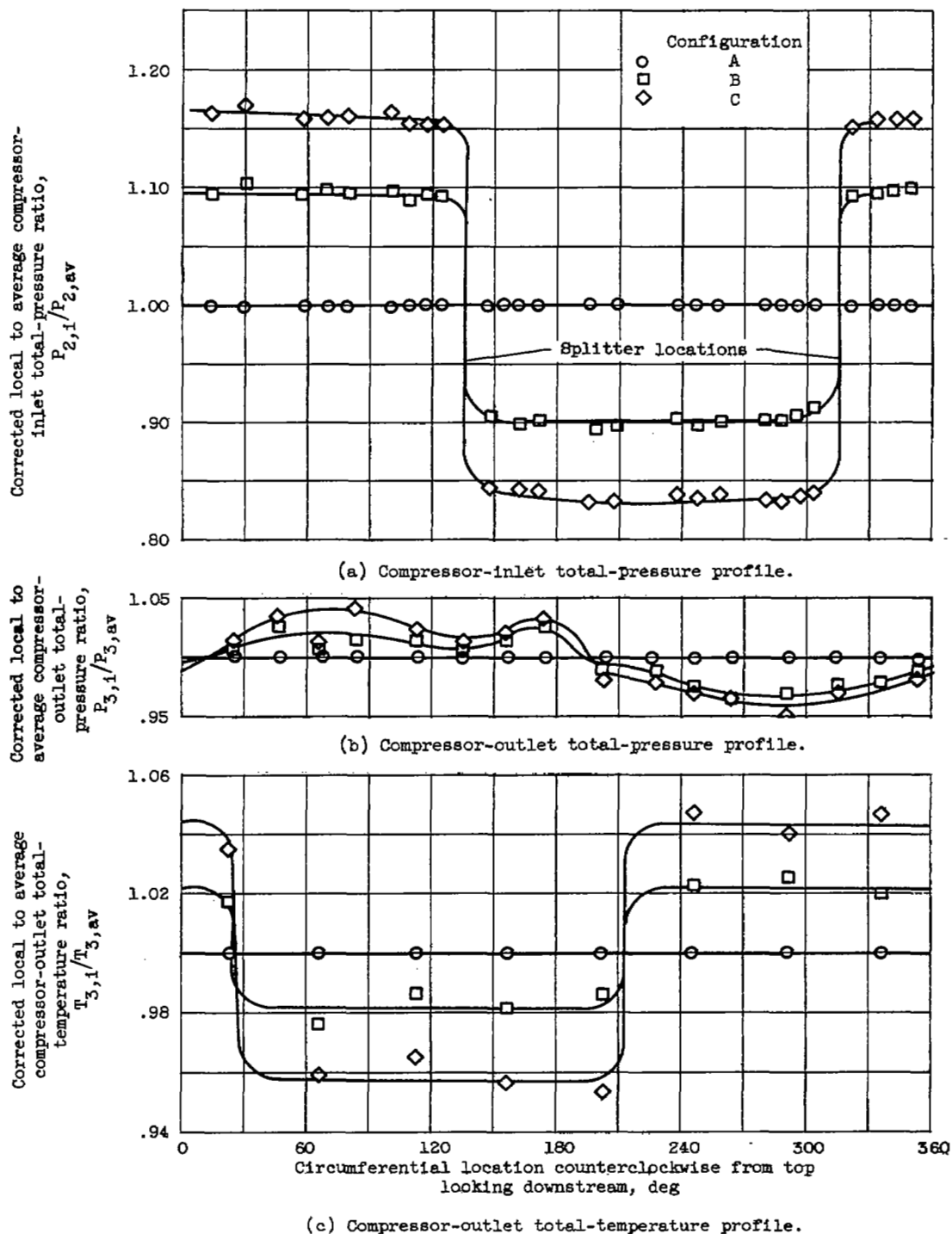
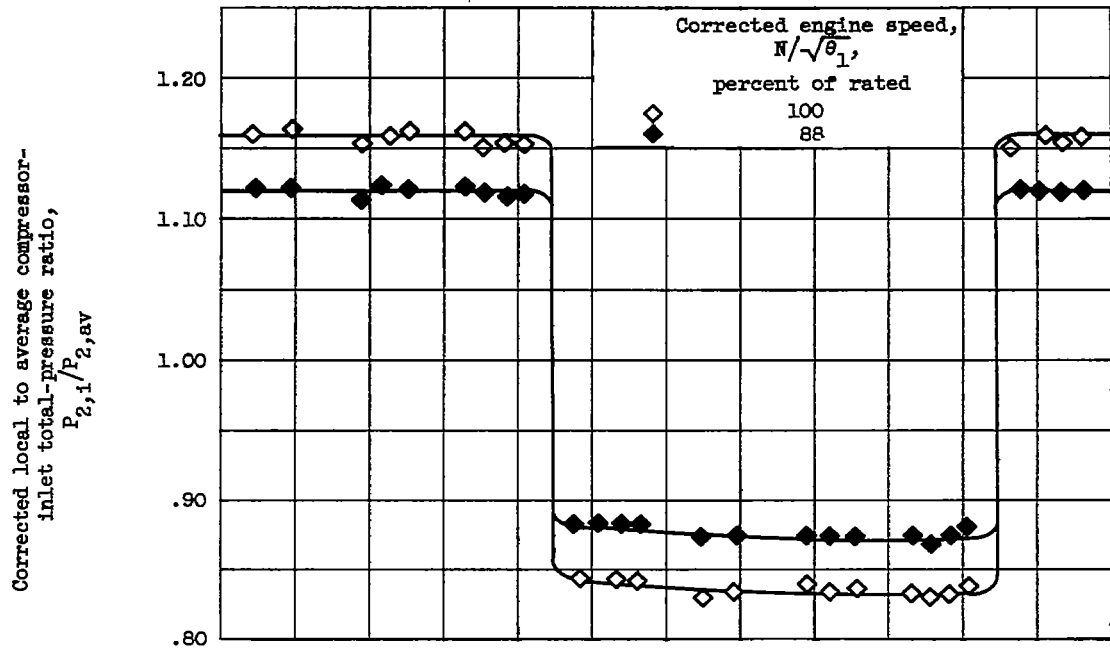


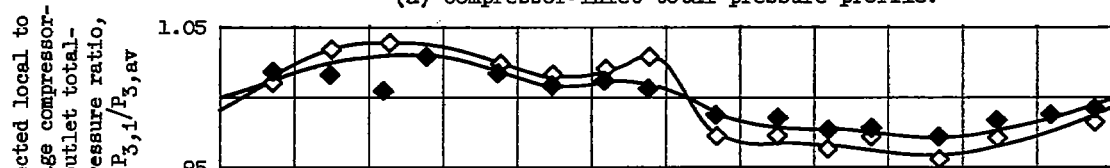
Figure 6. - Effect of air distortion on compressor pressure and temperature circumferential profiles. Corrected engine speed, $N/\sqrt{\theta_1}$, 100 percent of rated; Reynolds number index, 0.6.

3301

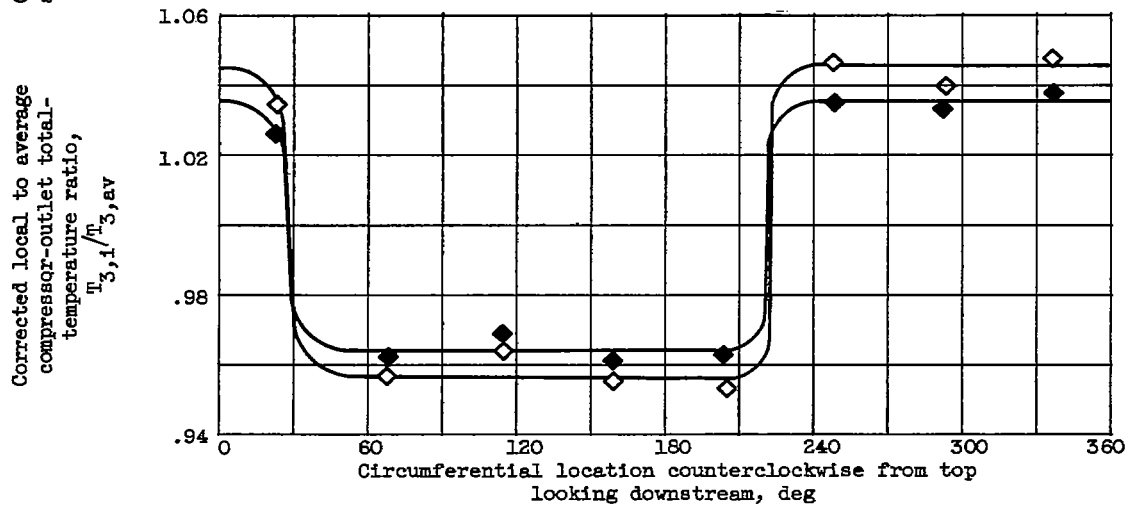
CR-4



(a) Compressor-inlet total-pressure profile.



(b) Compressor-outlet total-pressure profile.



(c) Compressor-outlet total-temperature profile.

Figure 7. - Effect of engine speed on compressor pressure and temperature circumferential profiles. Configuration C; Reynolds number index, 0.6.

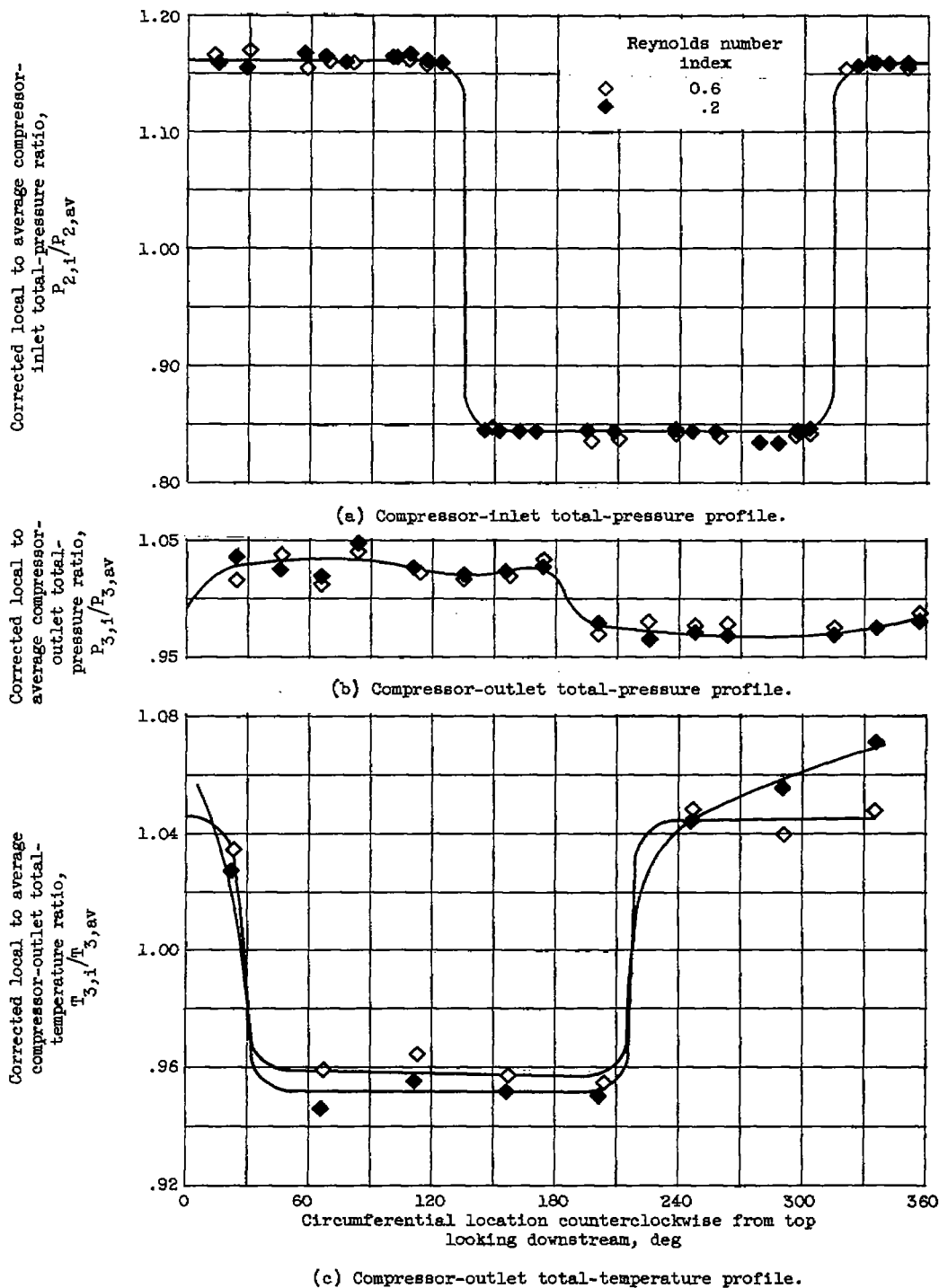


Figure 8. - Effect of Reynolds number index on compressor pressure and temperature circumferential profiles. Configuration C; corrected engine speed, $N/\sqrt{\theta_1}$, 100 percent of rated.

3301

CR-4 back

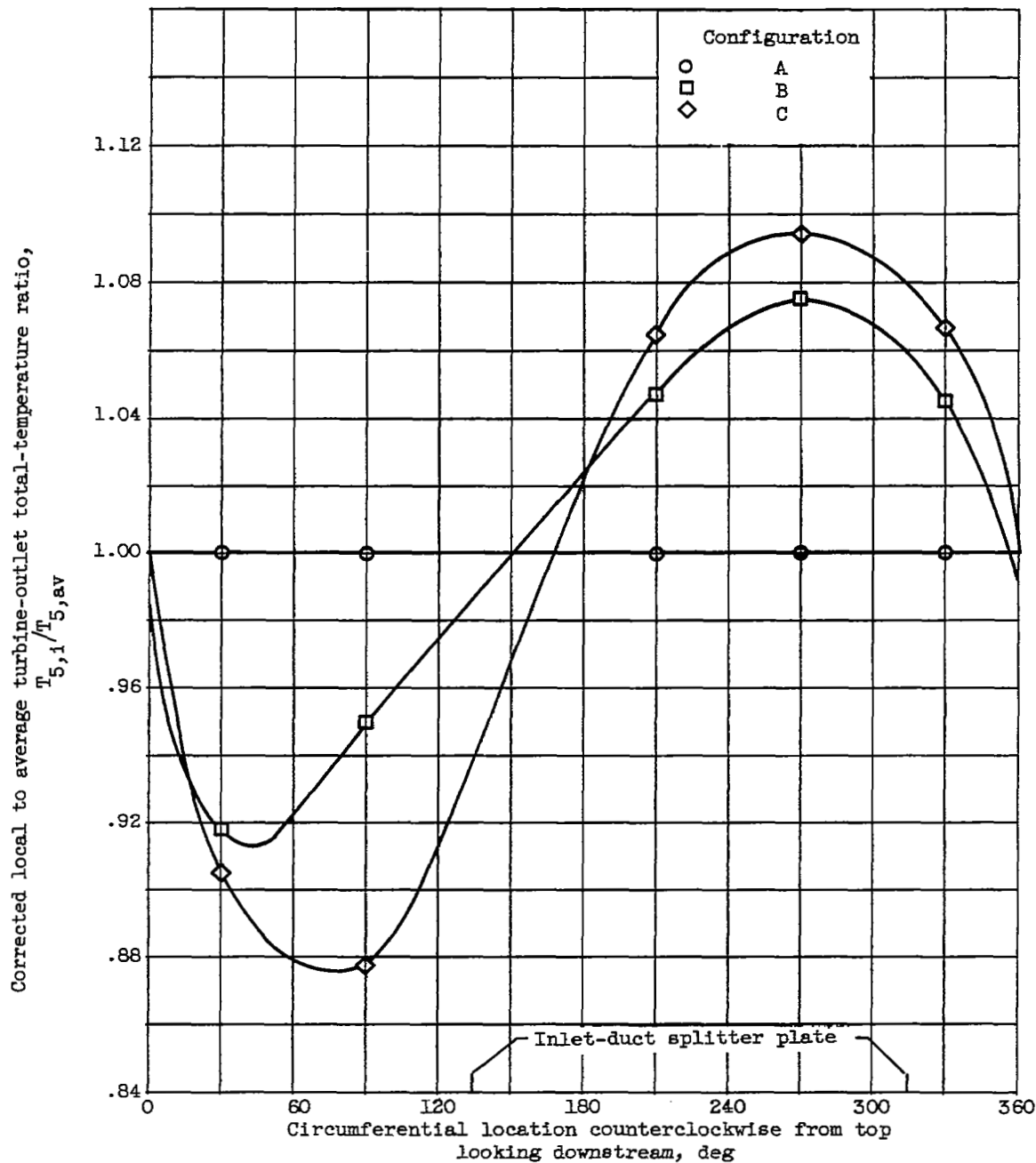
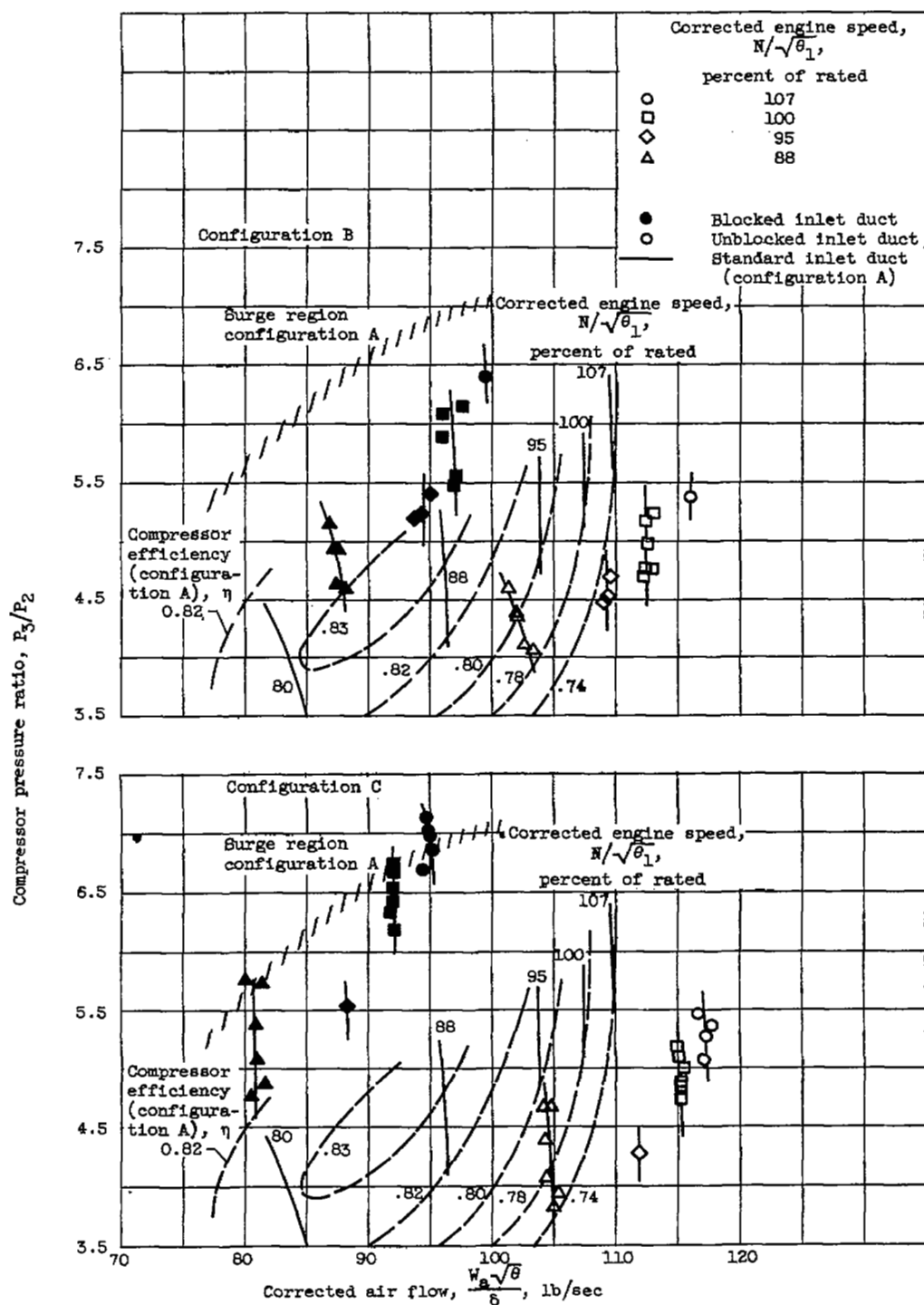


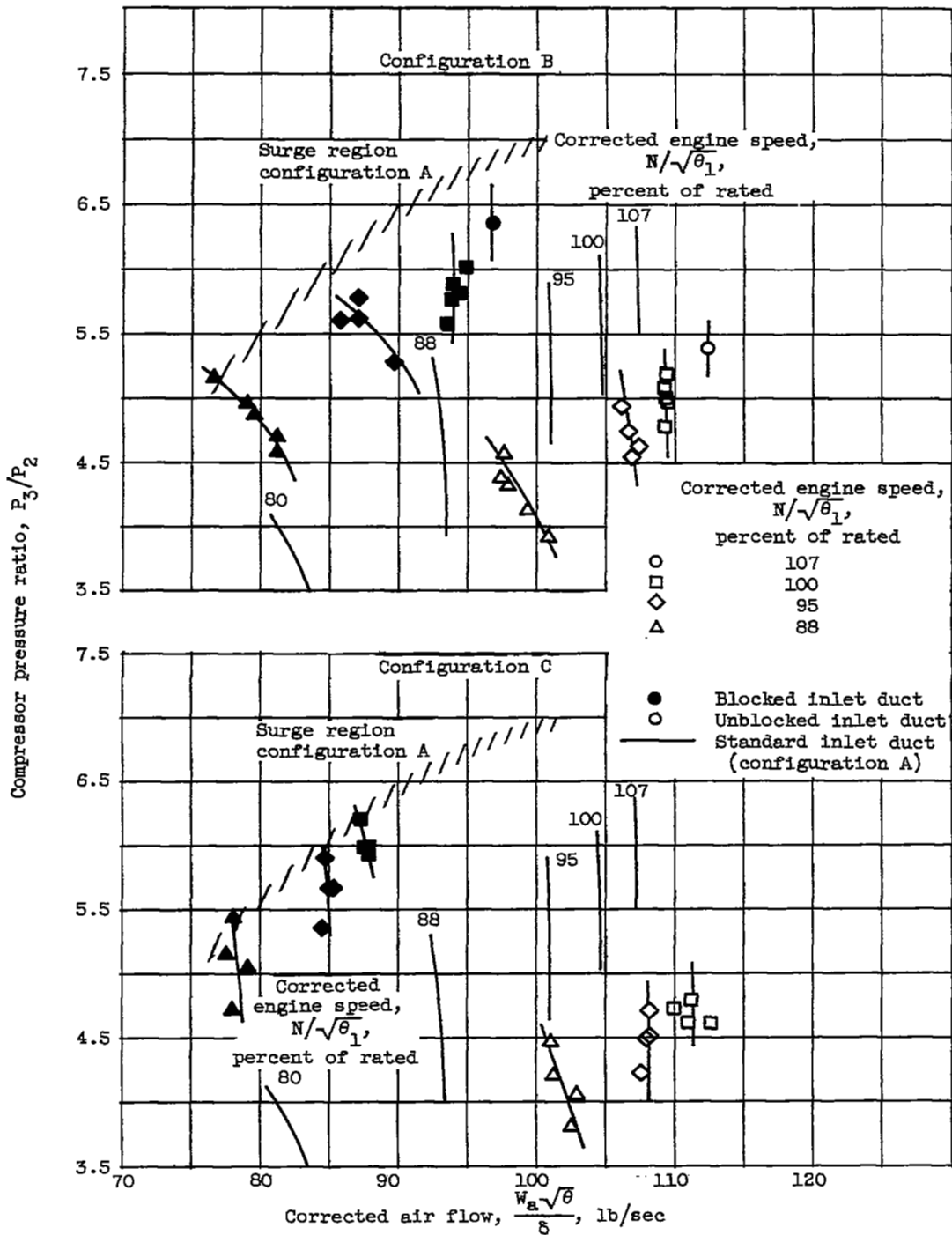
Figure 9. - Effect of inlet air distortion on turbine-outlet circumferential total-temperature profiles. Corrected engine speed, $N/\sqrt{\theta_1}$, 100 percent of rated. Reynolds number index, 0.6.



(a) Reynolds number index, 0.6.

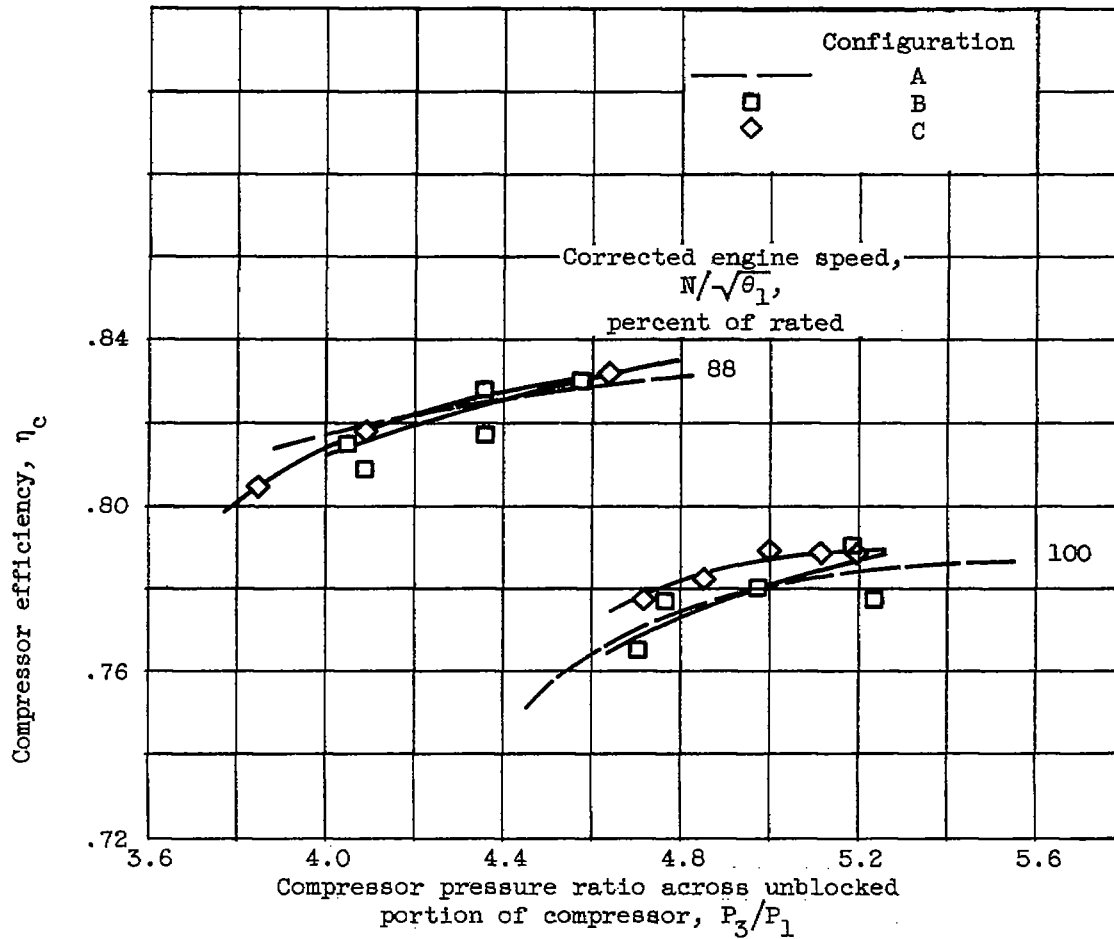
Figure 10. - Compressor characteristic lines for compressor based on air flow measured in each inlet duct.

3501



(b) Reynolds number index, 0.2.

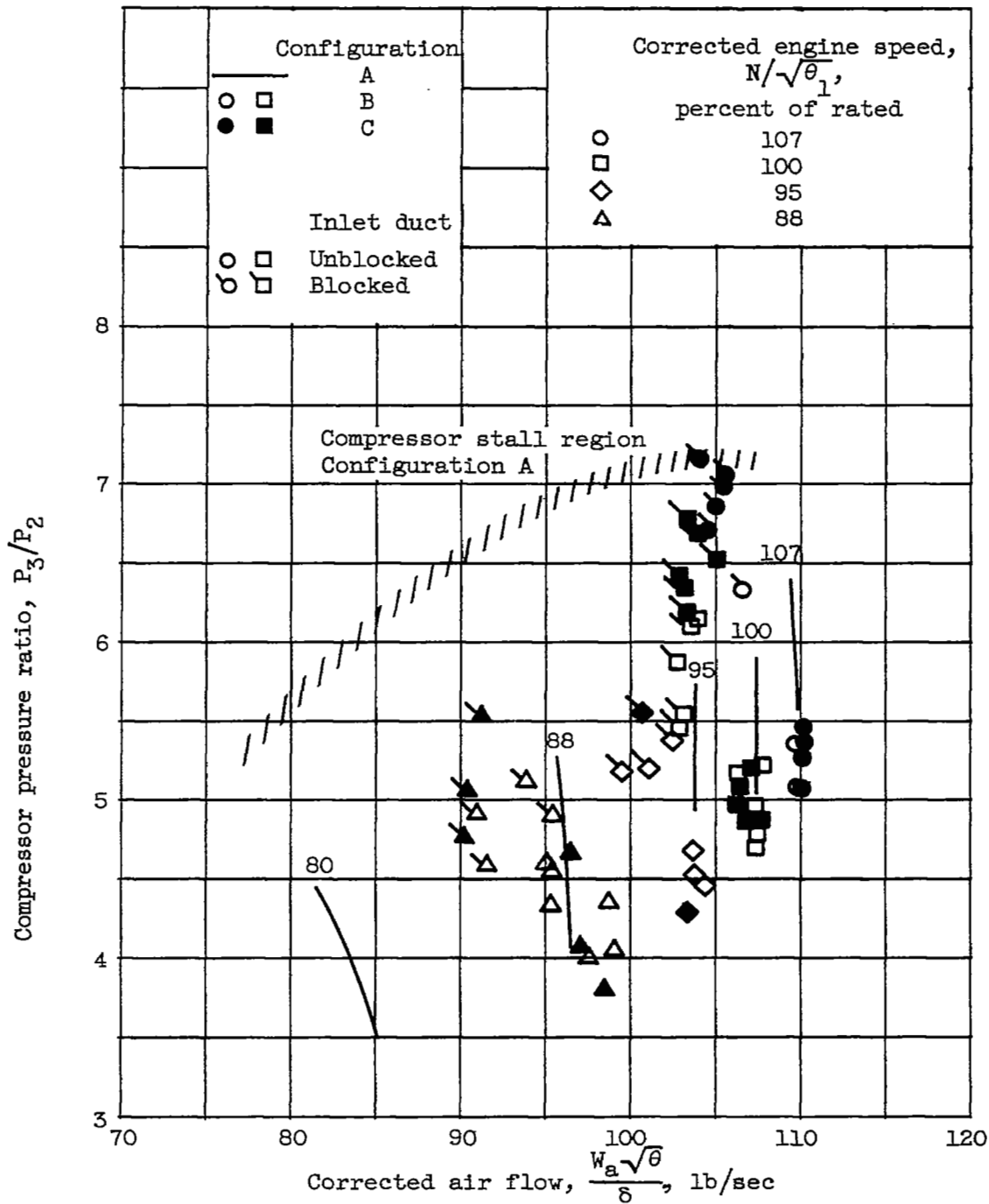
Figure 10. - Concluded. Compressor characteristic lines for compressor based on air flow measured in each inlet duct.



(a) Compressor efficiency for unblocked portion of compressor.

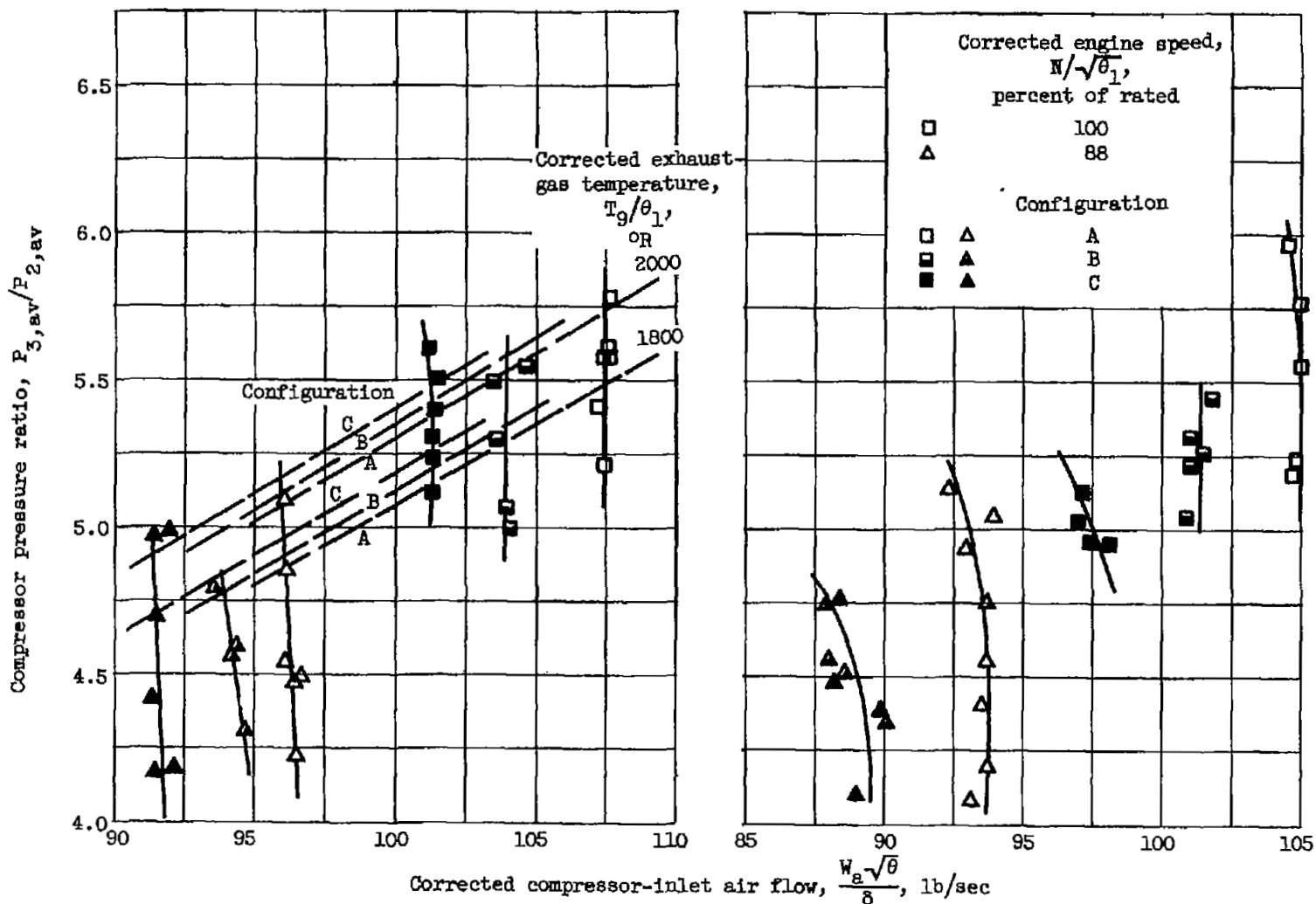
Figure 11. - Compressor performance based on adjusted air flow through each compressor half. Reynolds number index, 0.6.

3301



(b) Compressor characteristic lines.

Figure 11. - Concluded. Compressor performance based on adjusted air flow through each compressor half. Reynolds number index, 0.6.



(a) Reynolds number index, 0.6.

(b) Reynolds number index, 0.2.

Figure 12. - Compressor characteristic lines for over-all compressor performance.

3301

CR-5

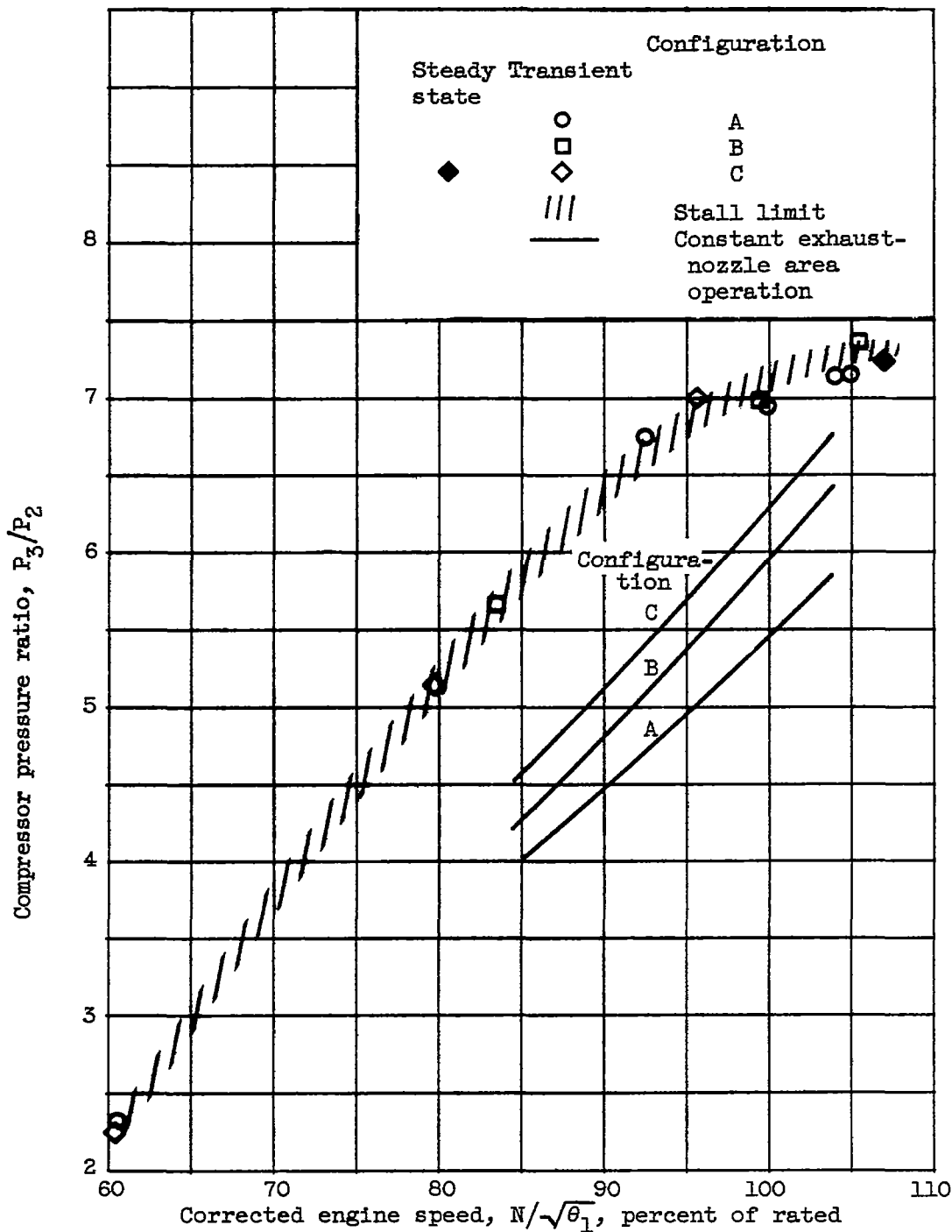
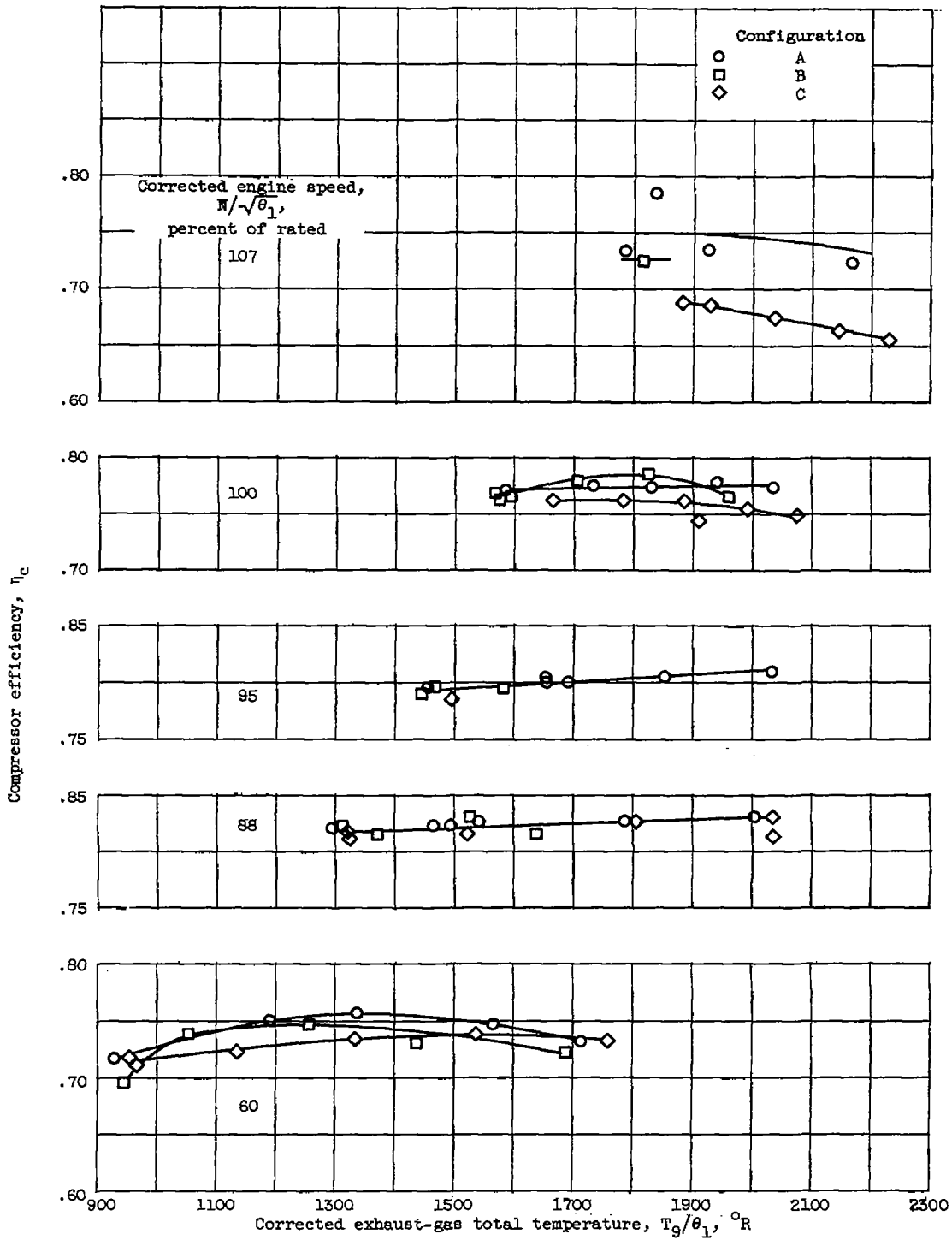


Figure 13. - Compressor stall limit without and with inlet air distortions based on compressor pressure ratio across blocked half of compressor. Reynolds number index, 0.6.

CONFIDENTIAL

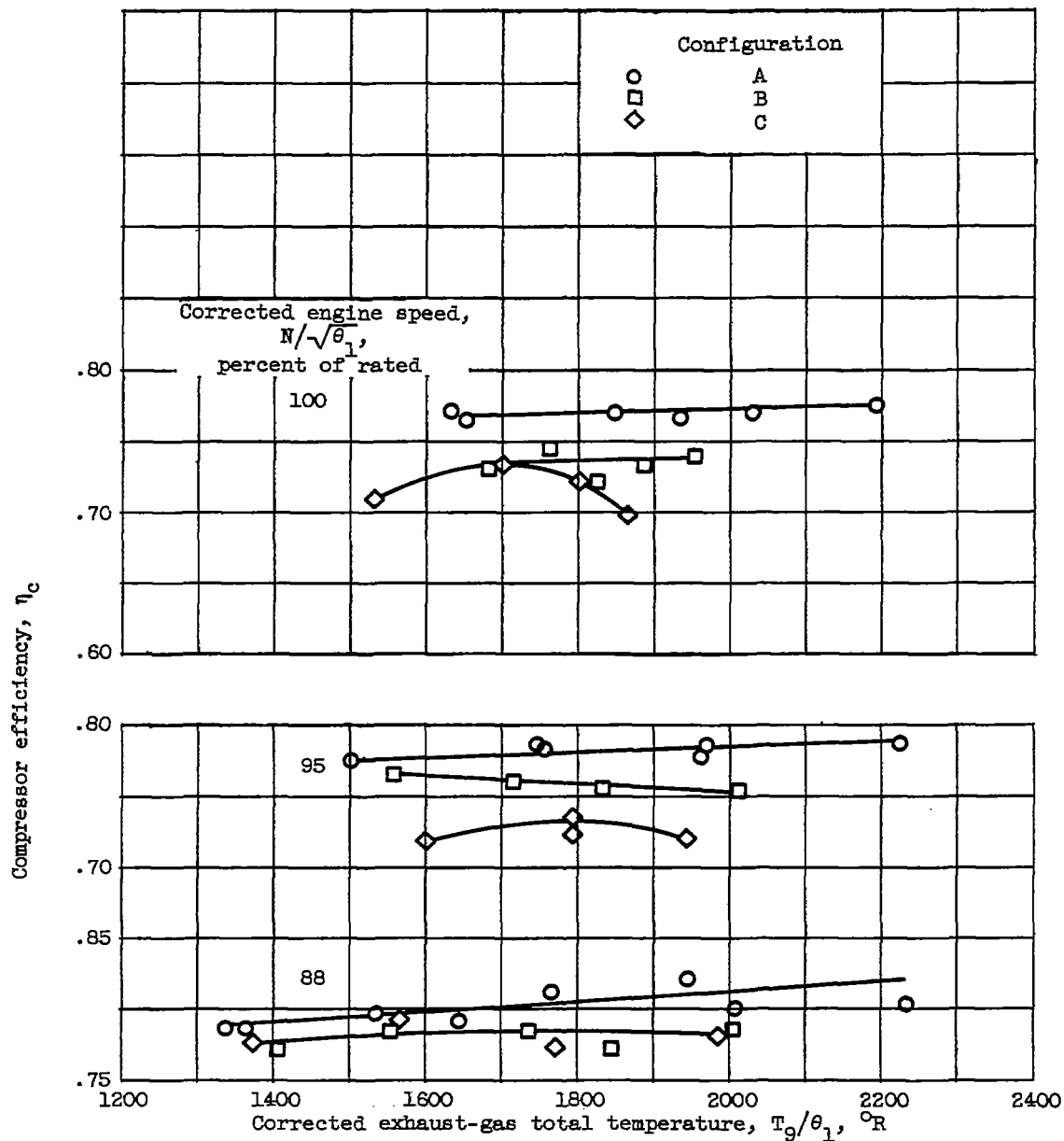


(a) Reynolds number index, 0.6.

Figure 14. - Effect of inlet-air distortion on over-all compressor efficiency.

3301

CR-5 back



(b) Reynolds number index, 0.2.

Figure 14. - Concluded. Effect of inlet-air distortion on over-all compressor efficiency.

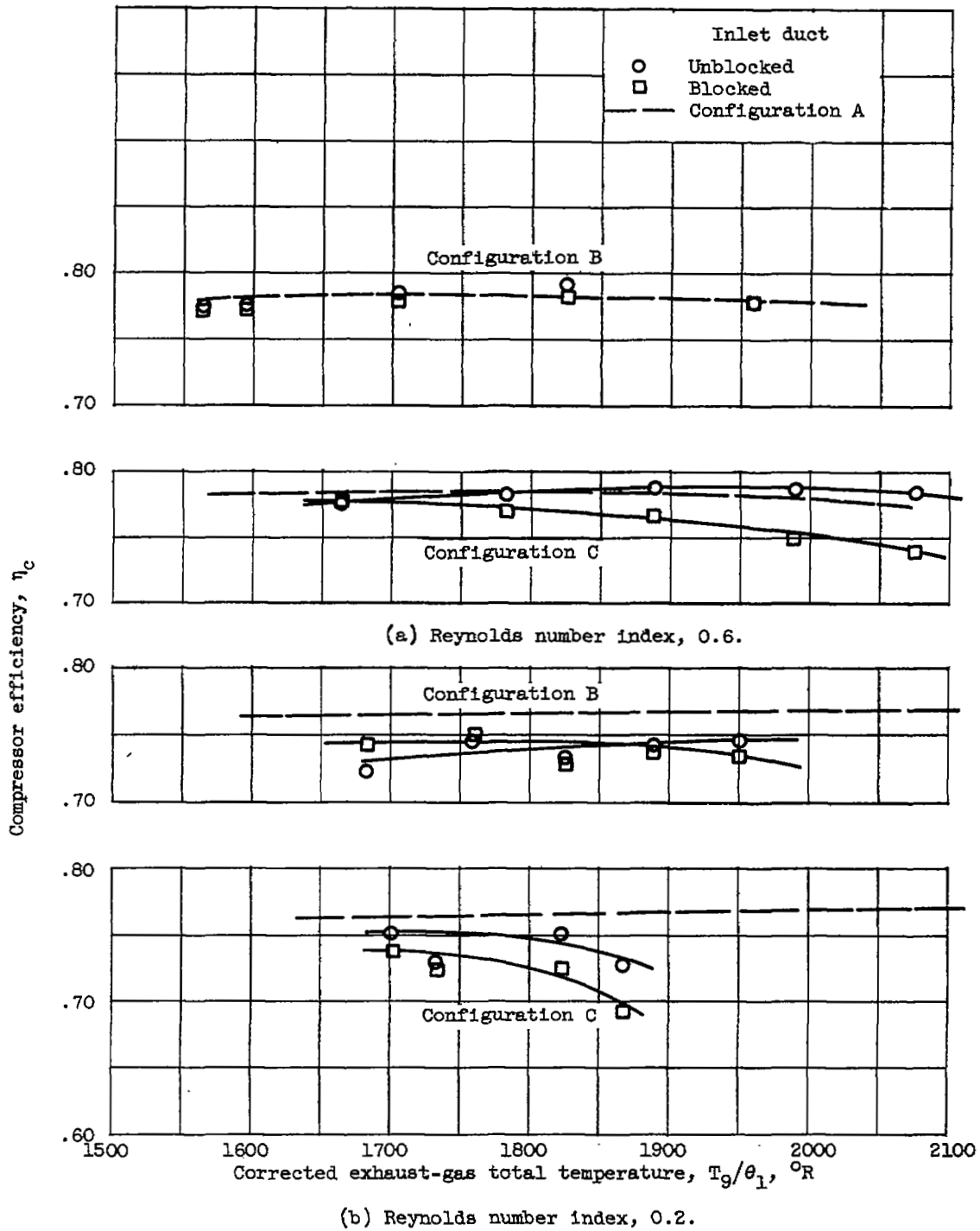
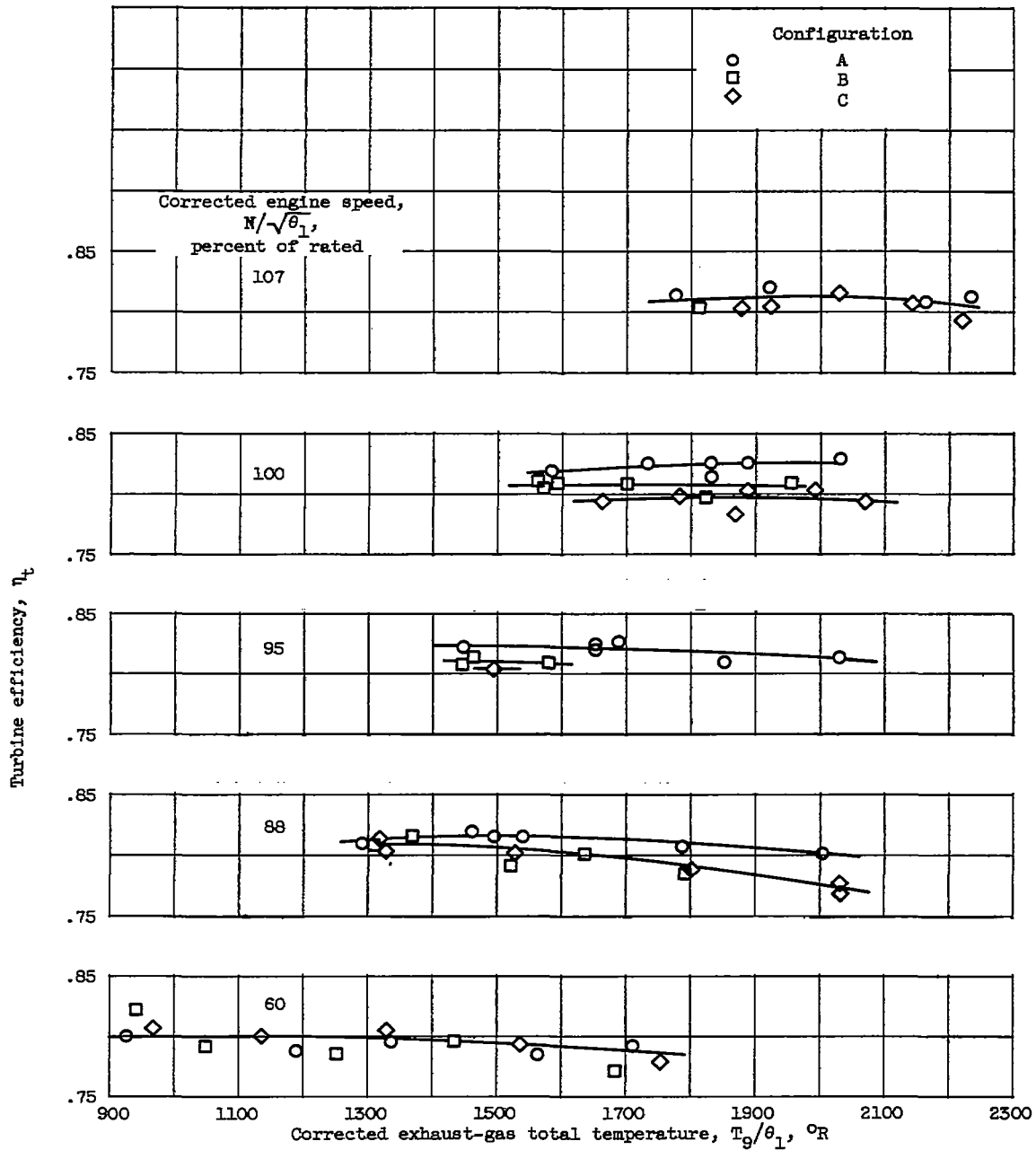


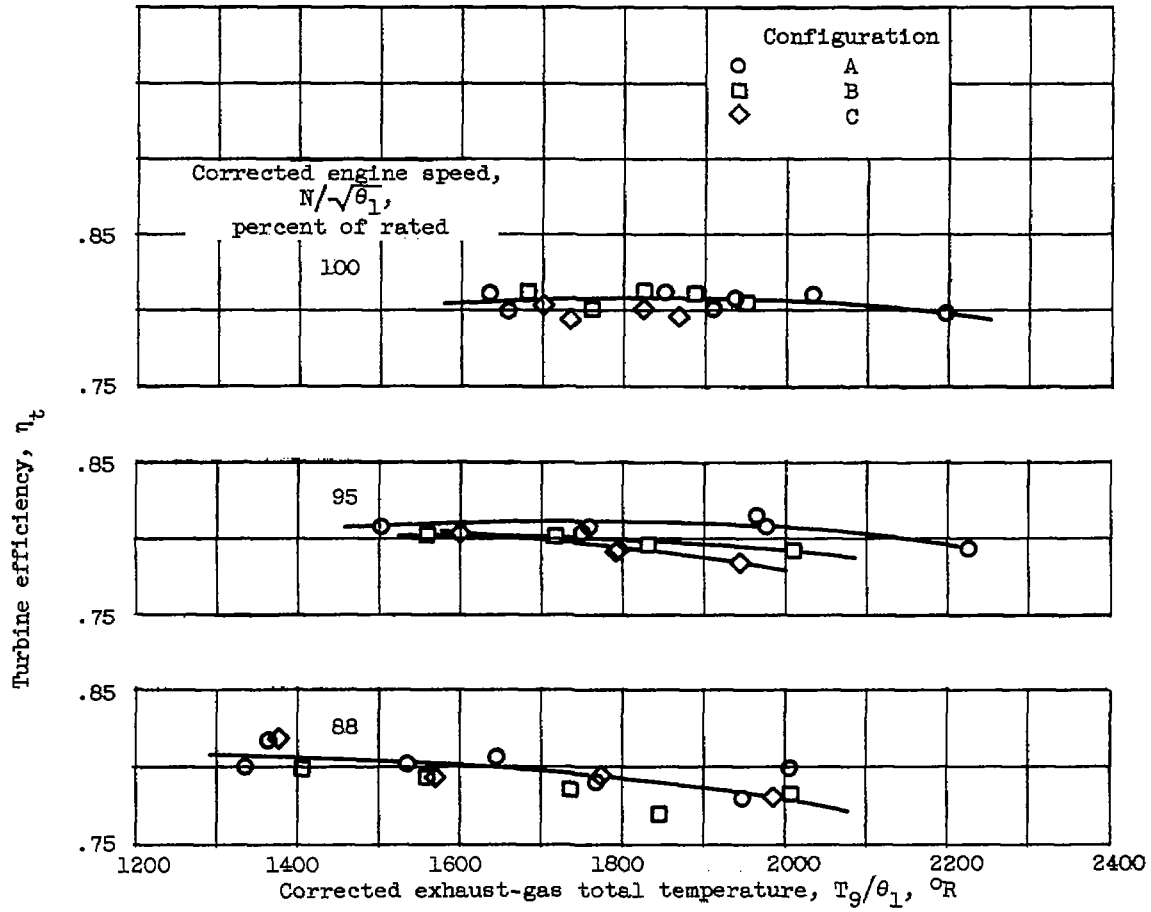
Figure 15. - Effect of inlet air distortion on compressor efficiency of each half of the compressor. Corrected engine speed, $N/\sqrt{\theta_1}$, 100 per cent of rated.

3301



(a) Reynolds number index, 0.6.

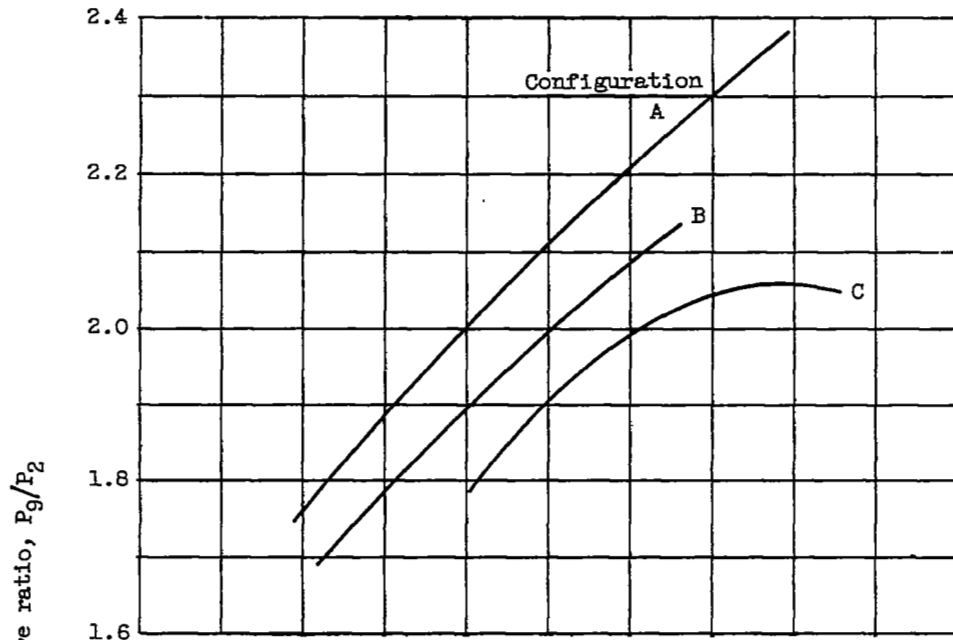
Figure 16. - Effect of inlet air distortion on turbine efficiency.



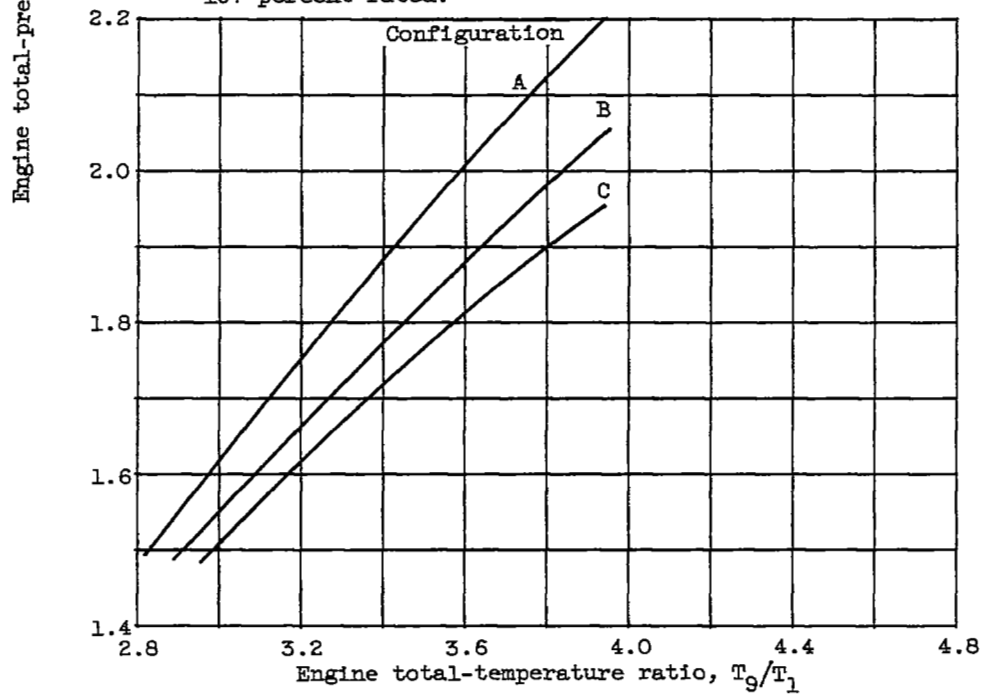
(b) Reynolds number index, 0.2.

Figure 16. - Concluded. Effect of inlet air distortion on turbine efficiency.

3301

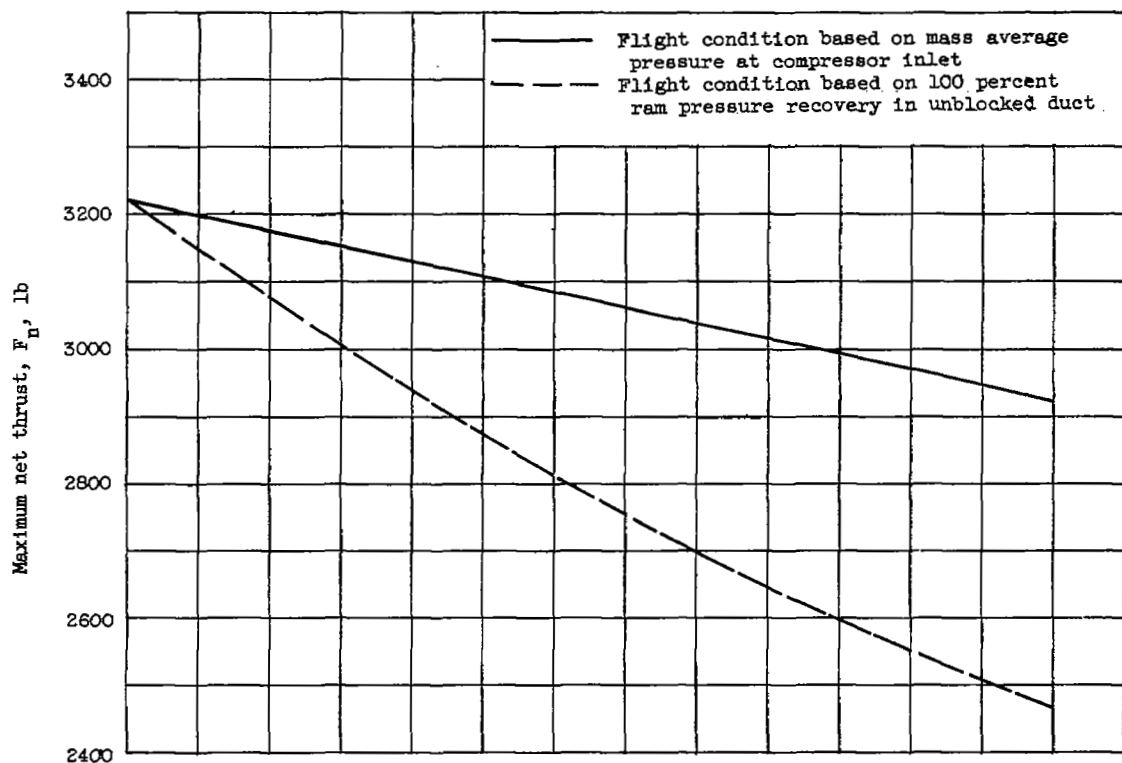


(a) Reynolds number index, 0.6; corrected engine speed, 107 percent rated.

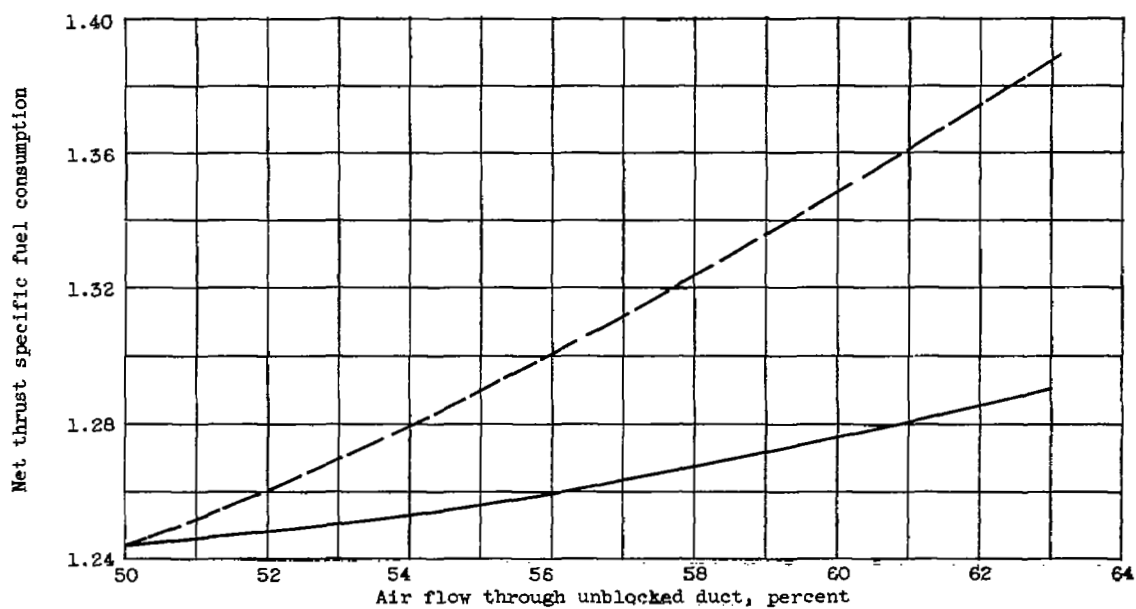


(b) Reynolds number index, 0.2; corrected engine speed, 100 percent rated.

Figure 17. - Effect of inlet air distortion on engine pumping characteristics.



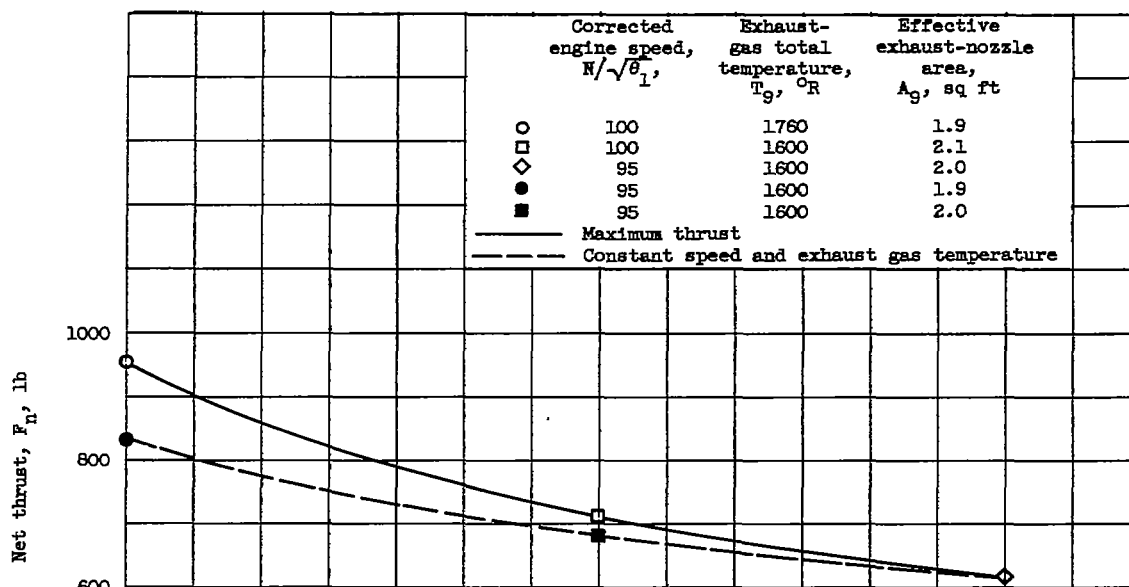
(a) Net thrust.



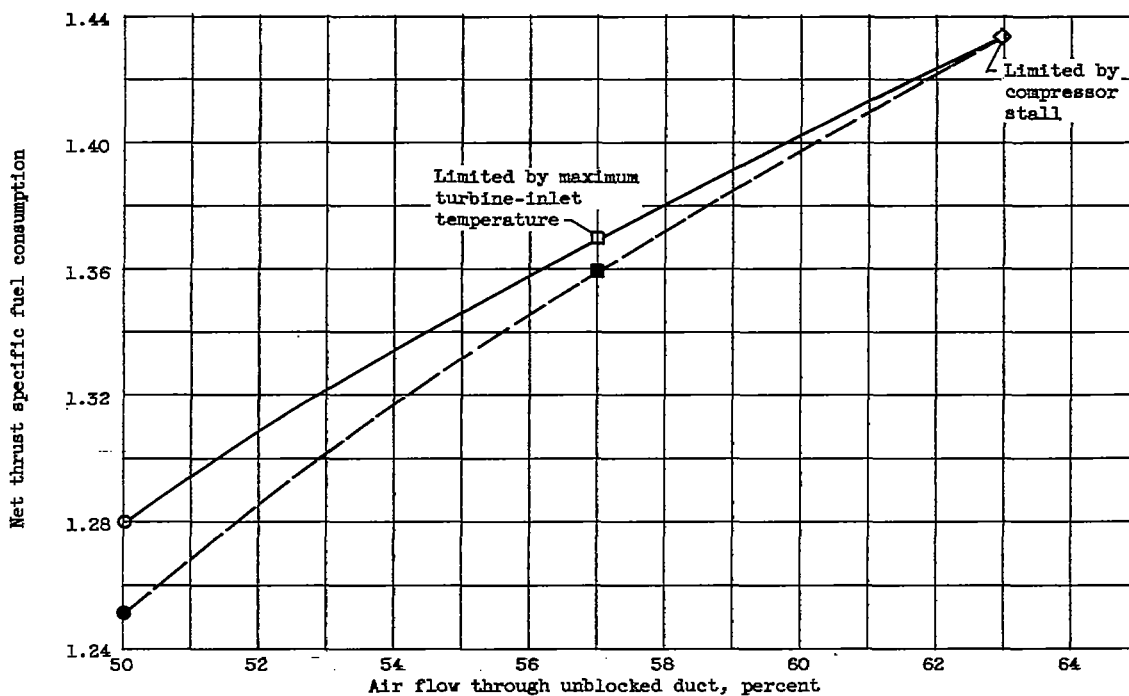
(b) Specific fuel consumption.

Figure 18. - Effect of inlet air distortion on net thrust and net thrust specific fuel consumption. Altitude, 22,000 feet; flight Mach number, 0.6; corrected engine speed, $N/\sqrt{\theta_1}$, 100 percent of rated; exhaust-gas temperature, T_g , 1760° R.

3301



(a) Net thrust.

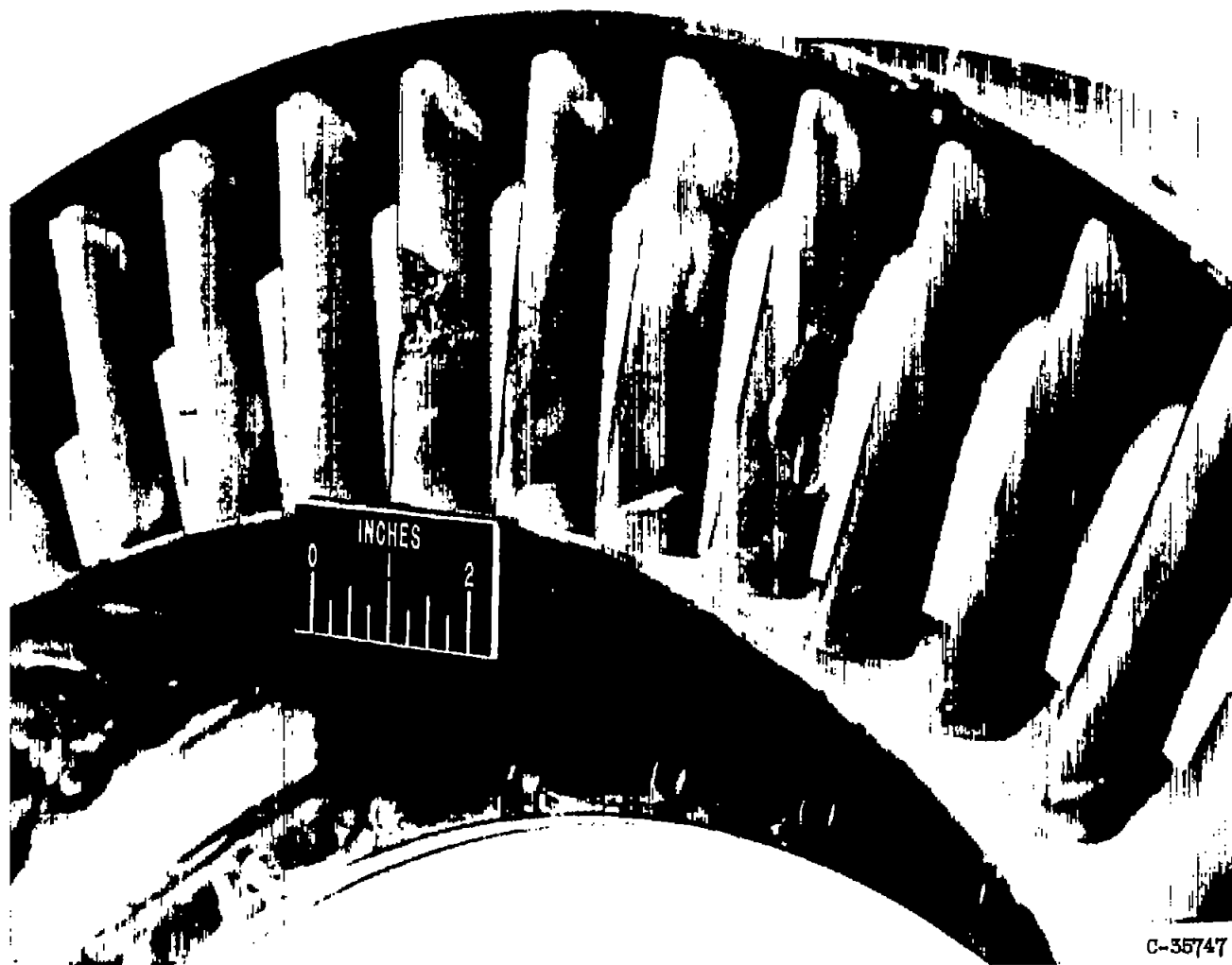


(b) Specific fuel consumption.

Figure 19. - Thrust derating required for stall-free compressor operation with inlet air division of 37:63 percent. Altitude, 50,000 feet; flight Mach number, 0.6.



Figure 20. - Oscillograph of rotating stall pattern at time of turbine failure.
Frequency, 56.3 cycles per second.



C-35747

(a) Upstream view of turbine stator.

Figure 21. - Turbine failure caused by air flow distortion.

3301

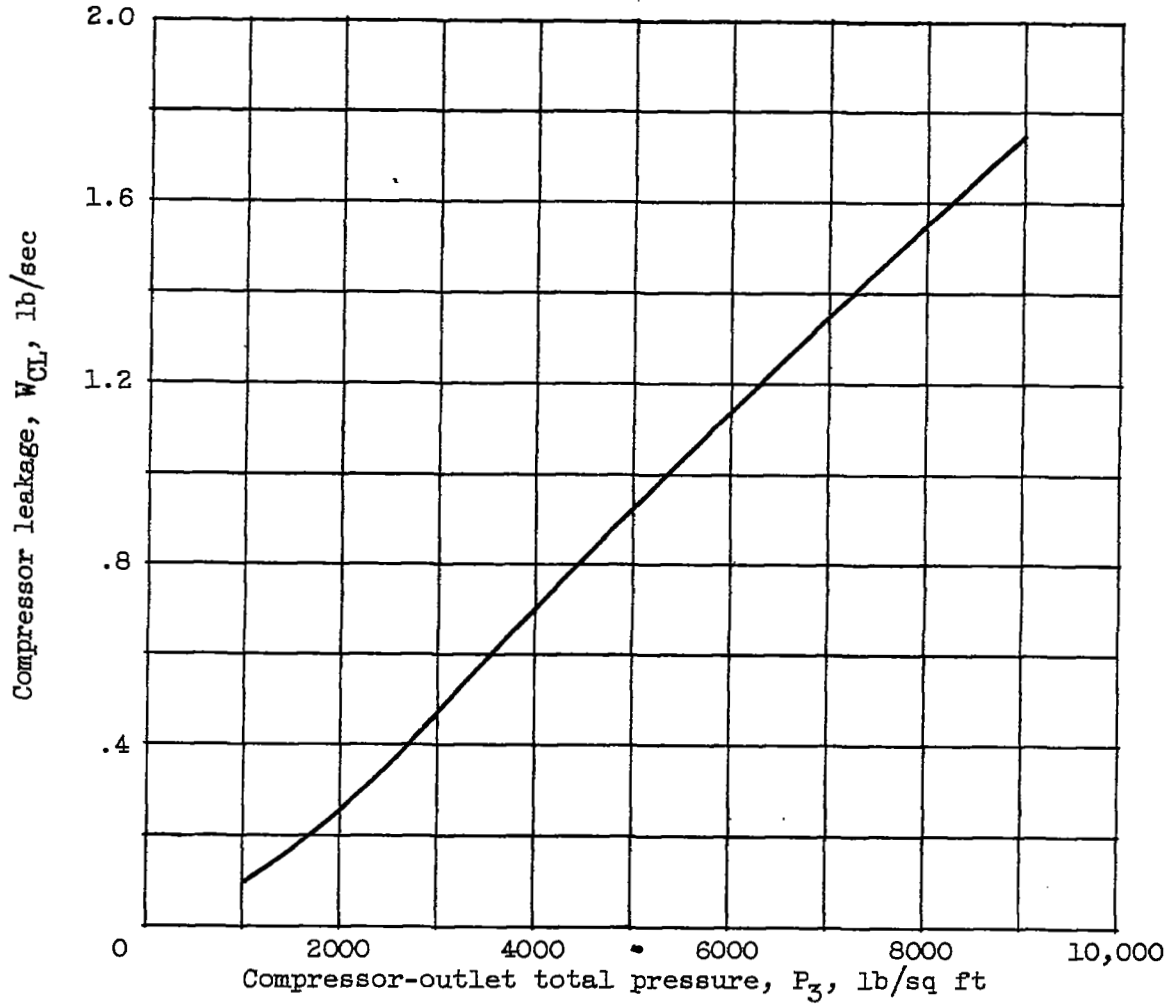


Figure 22. - Compressor leakage at engine midframe.

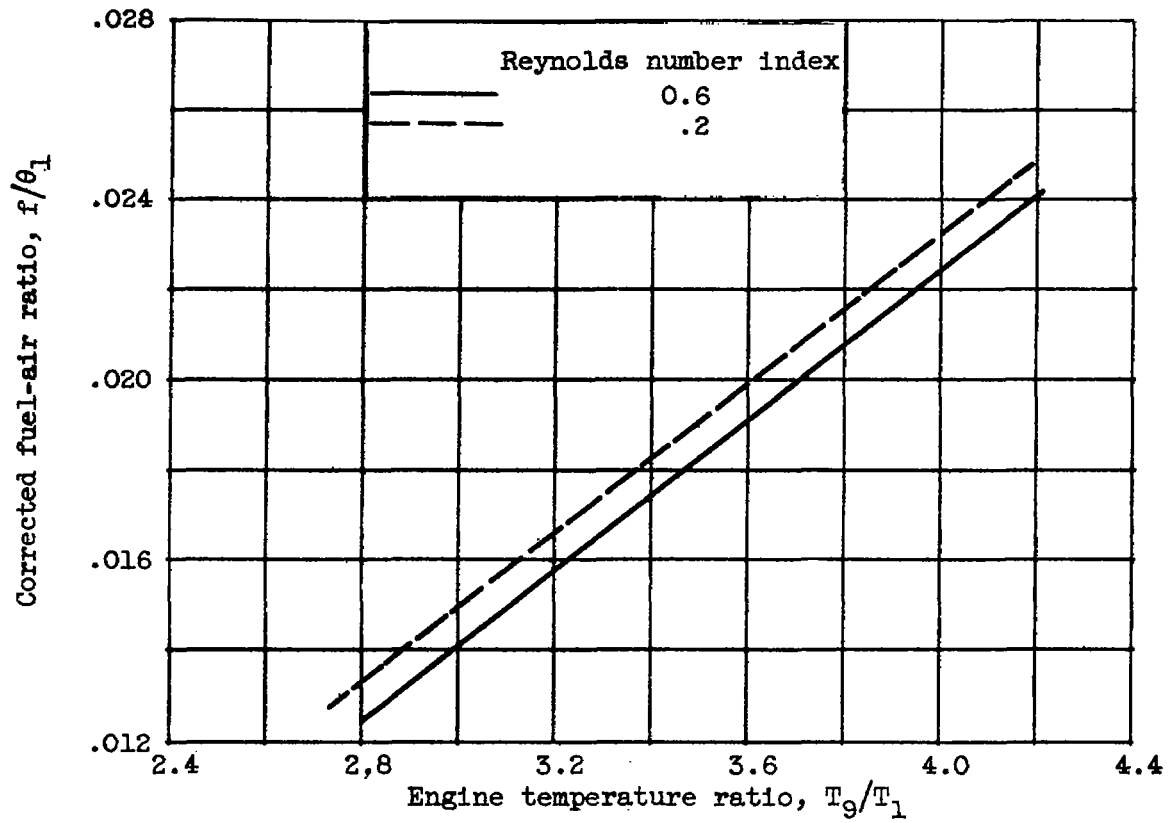


Figure 23. - Engine corrected fuel-air ratio.

NASA Technical Library



3 1176 01435 4089

